Scalar dark matter candidates revisited

Céline Bœhm,[1,*] Xiaoyong Chu[2,†] Jui-Lin Kuo[2,‡] and Josef Pradler[2,§]

[1]*School of Physics, Physics Road, The University of Sydney,*
New South Wales 2006 Camperdown, Sydney, Australia
[2]*Institute of High Energy Physics, Austrian Academy of Sciences,*
Nikolsdorfergasse 18, 1050 Vienna, Austria

We revisit the possibility of light-scalar dark matter, in the MeV to GeV mass bracket and coupled to electrons through fermion or vector mediators, in light of significant experimental and observational advances that probe new physics below the GeV scale. We establish new limits from electron colliders and fixed-target beams and derive the strength of loop-induced processes that are probed by precision physics, among other laboratory probes. In addition, we compute the cooling bound from SN1987A, consider self-scattering, structure formation, and cosmological constraints as well as the limits from dark matter–electron scattering in direct detection experiments. We then show that the combination of constraints largely excludes the possibility that the galactic annihilation of these particles may explain the long-standing International Gamma-Ray Astrophysics Laboratory excess of 511 keV photons as observed in the Galactic bulge. As a caveat to these conclusions, we identify the resonant annihilation regime where the vector mediator goes nearly on shell.

I. INTRODUCTION

The history of scalar dark matter (DM) in the MeV–GeV mass bracket is a long one. It has its roots when mainstream literature was primarily focusing on electroweak-scale new (supersymmetric) physics. High-energy colliders had long explored the GeV scale, and naive cosmological considerations suggested that thermal DM needed to have a mass of several GeV at the least [1,2]. However, light-scalar DM [3,4] turned out to be a perfect possibility—and still is. For example, it can couple to the Standard Model (SM) fermions either by a Yukawa-type interaction of some heavy fermions F or by a new gauge interaction mediated by a new vector particle Z' [4].

Cosmologically, such DM retained its right of existence by achieving a sufficient annihilation cross section through an equally light Z' (which has an even longer history [5,6]) or by a possible near independence of DM mass in the annihilation cross section when F is involved [4]. Experimentally, a light Z' was viable, because the neutral

current phenomenology remained largely unaffected, either from a suppression with center-of-mass energy arising from momentum-resolved diagrams in processes at high energy or, at low energy, by ensuring that the effective strength of the interaction is smaller than the weak interactions of the SM. In turn, a model with F mediation was even simpler to retain, as the mass scale of these particles can be in the TeV range.

This, at the time, seeming "niche physics" quickly gained momentum. When the spectrometer on board the International Gamma-Ray Astrophysics Laboratory (INTEGRAL) satellite confirmed a strong flux of 511 keV photons at the level of almost 10^{-3} /cm^2/s [7,8] (see also [9,10]) coming from the Galactic bulge, a MeV-scale DM origin was suggested on the basis of its spatial morphology and its general compatibility with the relic density requirement [11] while at the same time obeying soft gamma-ray constraints [3,12,13]. Concretely, the signal, especially its high bulge-to-disk ratio, is unexpected from known astrophysics [9,14] and calls for a new production mechanism of low-energy positrons. This can be achieved through DM annihilation into e^+e^- pairs.

The second piece of early impetus for such models was their connection to low-energy precision physics, in particular, to the electron and muon anomalous magnetic moments $(g-2)_{e,\mu}$. There is a curious coincidence between the DM-viable parameters of the models, in part suggested by Eq. (1), and the lepton-mass-dependent shifts to $(g-2)_{e(\mu)}$ on the order of 10^{-11} (10^{-9})—essentially at

*celine.boehm@sydney.edu.au
†xiaoyong.chu@oeaw.ac.at
‡jui-lin.kuo@oeaw.ac.at
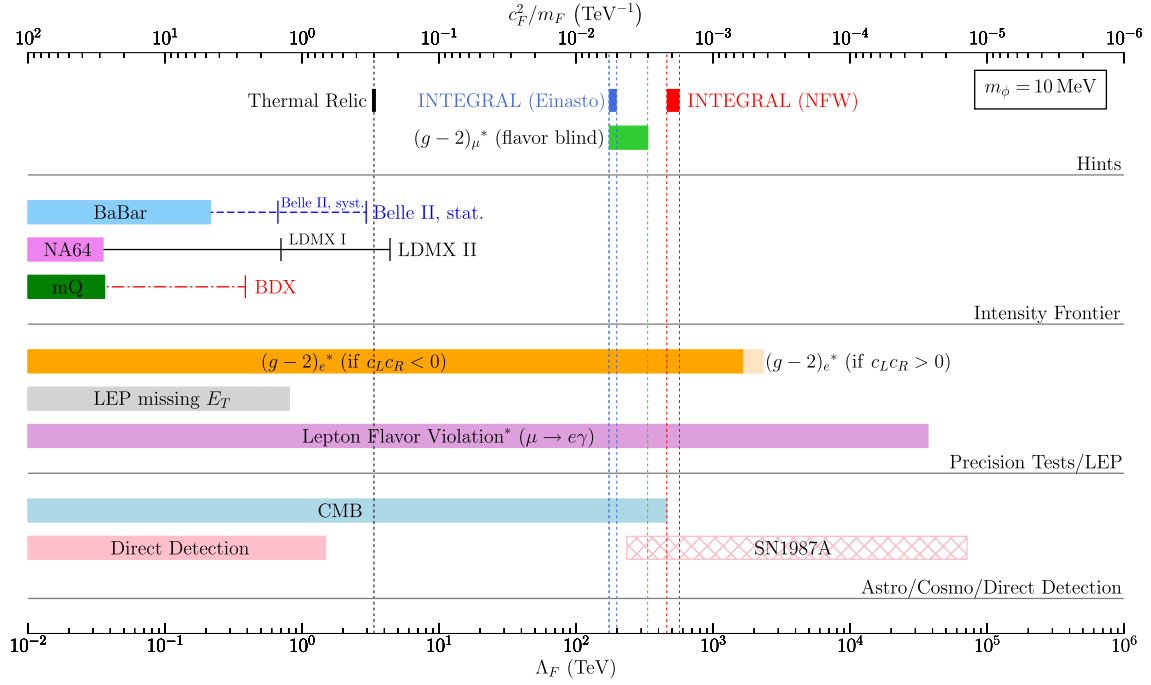§josef.pradler@oeaw.ac.at

FIG. 1. Summary of constraints obtained in this paper for the fermion-mediated model as a function of the effective UV-scale $\Lambda_F = (c_F^2/m_F)^{-1}$ for a fixed DM mass of $m_\phi = 10$ MeV in the heavy mediator limit; $c_F = \sqrt{|c_L^e c_R^e|}$. A star indicates that the bound applies only under certain conditions. The top section "hints" shows the regions of interest for the explanation of the INTEGRAL signal, for the $(g-2)_\mu$ anomaly assuming flavor-blind couplings and the same F masses between the first two generations, and the point for achieving the correct relic density through DM freeze-out. The next section "intensity frontier" shows constraints (projections) from searches for missing momentum in e^+e^- collisions at *BABAR* (Belle II), for missing energy in the e^- fixed-target experiment NA64 (LDMX), and for direct $\phi-e^-$ scattering of ϕ produced in the e^- fixed-target experiment mQ (BDX). The section "precision tests/LEP" shows the conservative constraint from the loop-induced contribution to $(g-2)_e$ for either sign of the product of couplings as labeled [32,33], the limit on missing energy searches at LEP, and, in the case of a single generation of F and assuming flavor-blind couplings, the limit from the lepton-flavor-violating $\mu \to e\gamma$ transition. The final section "astro/cosmo/direct detection" is devoted to CMB limits on energy injection, to direct detection limits from ϕ-electron scattering and from anomalous energy loss in SN1987A. Weaker limits such as from the invisible width of the Z, from structure formation, from DM self-scattering, from the running of α, and from the left-right asymmetry in polarized electron-electron scattering are not shown (see the main text instead). The INTEGRAL interpretation is excluded.

the level of their observed magnitudes [11].[1] This is a nice example of how laboratory probes of SM quantities inform us on the astrophysical and cosmological viability of new physics and vice versa [16].

A lot of general phenomenological progress has been made since the introduction of the aforementioned scalar DM models. Regarding the INTEGRAL interpretation, the DM mass is now strongly constrained, e.g., from annihilation in flight, and the DM mass now generally needs to be below tens of MeV and can even be fully excluded in specific models and/or under certain assumptions of the state of the early Universe; for more details, see, e.g., [3,12,17,18], and references therein. In turn, the measurement [19] of the anomalous magnetic moment of the muon now stands in $(3-4)\sigma$ tension with the SM predicted one [20]. In fact, the imminent experimental update for $(g-2)_\mu$

is much in the limelight today, especially after its connection with GeV-scale dark sector physics became more broadly appreciated following Ref. [21]. Finally, a beyond the Standard Model (BSM) sector that contains light dark states has found further motivations, such as the astrophysical core-cusp problem [22–24] and various galactic cosmic ray excesses [25–28], among others. These motivations paired with the to-date absence of new physics at the electroweak (EW) scale have acted as a great innovation driver for devising laboratory and observational tests for sub-GeV dark sector physics; see, e.g., Refs. [29–31], and references therein.

In light of the significant amount of activities in the past two decades that has gone into the exploration of the MeV–GeV mass range and the large amount of results, it seems timely to revisit the originally proposed models of sub-GeV scalar DM [4] and confront them with this new wealth of data. Concretely, we add the following new pieces that were not presented previously in this context:

---

[1]The more general phenomenology of a light Z', including coupling to quarks, was originally considered in Refs. [5,6,15].
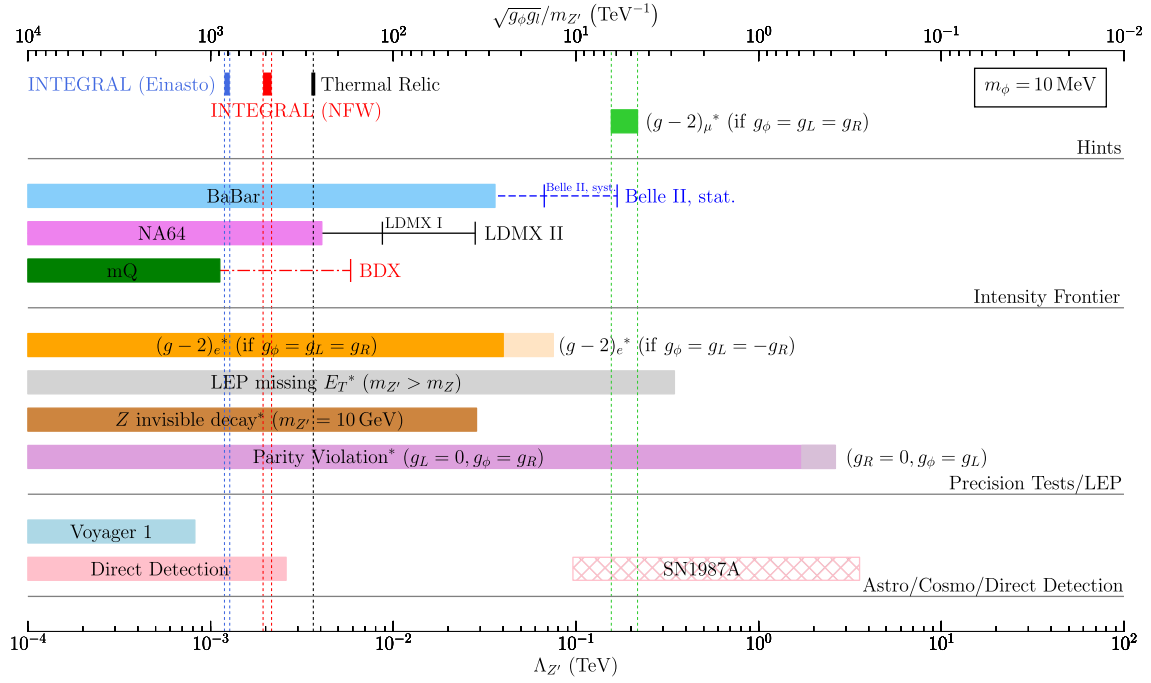
FIG. 2. Summary of constraints obtained in this paper for the vector-mediated model as a function of the effective scale $\Lambda_{Z'} = (\sqrt{g_\phi g_l}/m_{Z'})^{-1}$ for a fixed DM mass of $m_\phi = 10$ MeV in the heavy mediator limit, similar to Fig. 1. A star indicates that the bound applies only under certain conditions. The new or additionally shown bounds here are from the Z-invisible width (for $m_{Z'} = 10$ GeV only) and from parity violation using E158 under the assumption $g_\phi = g_L$ in the section precision tests/LEP. Section astro/cosmo/direct detection now shows the annihilation constraint from *Voyager 1* data. The region of interest for $(g-2)_{e,\mu}$, where the bound for $(g-2)_e$ is based on Refs. [32,33], also requires further assumptions of couplings $g_\phi = g_L = \pm g_R$. The INTEGRAL interpretation is excluded.

(i) Sensitivities of current and future intensity-frontier experiments are derived for the first model and revisited for the second;

(ii) in addition to an update of the $g-2$ constraint from electrons, limits from lepton flavor violation, parity violation, and the invisible decay of the Z boson are established;

(iii) the astrophysical cooling constraint from SN1987A is derived in detail for both the free-streaming and trapping regimes;

(iv) the bound from astrophysical DM self-scattering is derived, while we adopt the limits on DM annihilation at the cosmic microwave background (CMB) epoch and from *Voyager 1* data at the present time in the literature;

(v) the high-redshift constraint from the collisional damping of DM primordial fluctuations is considered and from extra radiation degrees of freedom is revisited;

(vi) latest constraints from the leading direct detection experiments are summarized to apply to the models;

(vii) the sensitivity of the high-energy colliders, Large Electron-Positron collider (LEP) and LHC, is provided;

(viii) an improved velocity expansion for the annihilation cross section for one of the models is presented.

Taken together, this will provide a more comprehensive assessment as to whether light dark matter particles could explain INTEGRAL or the anomalous magnetic moment of the muon in this setup. It is important to stress, however, that, although these anomalies serve as good and timely motivations, our study has the broader aspect that it presents a complete and self-contained survey on the viability of rather minimal models of scalar DM below the GeV scale. A summary of results for an exemplary DM mass of 10 MeV is shown in Figs. 1 and 2.

The paper is organized as follows: In Sec. III, we introduce the models together with the parameter regions of central interest. In Sec. IV, the bounds from the intensity-frontier experiments, from precision observables, and from LEP are derived. While such bounds constrain parts of the parameter regions of interests, complementary limits arise from cosmological and astrophysical observations, discussed in Sec. V. Section VI is devoted to a study of the low mediator mass region in the Z' model. Conclusions are presented in Sec. VII. Several Appendixes provide additional details on our calculations.

II. STATUS OF THE INTEGRAL LINE

Before we go into the specifics of the scalar DM models, for self-completeness, in this section we provide a lighting

review on the status of the INTEGRAL line in its connection to annihilating DM into e^+e^- pairs. Decomposing the annihilation cross section in terms of the relative velocity as $\sigma_{\mathrm{ann}}v = a + bv^2$ and assuming a Navarro-Frenk-White (NFW) dark matter halo profile, the observations suggest that the best fit values for the a or b parameters are [16], respectively,

$$a \simeq 2.2 \times 10^{-31} \left(\frac{m_\phi}{\mathrm{MeV}}\right)^2 \mathrm{cm}^3\,\mathrm{s}^{-1}, \qquad (1a)$$

$$b \simeq 3.4 \times 10^{-25} \left(\frac{m_\phi}{\mathrm{MeV}}\right)^2 \mathrm{cm}^3\,\mathrm{s}^{-1}, \qquad (1b)$$

with a strong preference for a constant cross section (a value) [34] albeit large uncertainties and an additional dependence on the cuspiness of the inner DM halo profile [35]. With these numbers in mind, the p wave is roughly commensurate with the value required for a successful thermal relic $\sigma_{\mathrm{ann}}v \sim$ few $\times 10^{-26}$ cm^3 s^{-1} (where $v \sim 0.3$ at freeze-out).

The question of viable DM mass is an involved one. The injected positrons produced in DM annihilation need to decelerate to nonrelativistic speeds before annihilating to explain the 511 keV INTEGRAL line. Because of substantial uncertainties in astrophysical propagation modeling [36,37], the maximal DM mass that can explain the line remains uncertain; see [38] for a recent summary. There are, however, several quantitative results with regard to spectral features.

(i) Extra photons created by bremsstrahlung in the annihilation process suggest $m_\phi \lesssim 20$ MeV [12], although more detailed calculations relax this bound to $m_\phi \lesssim$ 30–100 MeV [17]. This is comparable to the *Voyager 1* bound based on local $e^\pm$ measurements [39].

(ii) The most stringent constraint on the DM mass is obtained when considering the in-flight annihilation, implying $m_\phi \lesssim$ 3–7.5 MeV [40,41], mostly from the COMPTEL diffuse γ-ray background measurements. The constraint is derived from the x-ray background inside the gas-dense region of the Galactic Center.

(iii) Recently, Ref. [42] has revisited the extra photon emission (mainly via inverse Compton scattering) from DM annihilation at higher latitudes, where in-flight annihilation is subleading. Such treatment leads to a much weaker bound from the INTEGRAL data, $m_\phi \lesssim 70$ MeV, when normalizing on the 511 keV line strength. Furthermore, Ref. [43] considers both bremsstrahlung and in-flight annihilation, showing that a future e-ASTROGAM experiment is able to probe the DM mass down to 4 MeV.

III. REPRESENTATIVE MODELS

In this paper, we shall focus on a complex scalar DM candidate. The Galactic 511 keV gamma-ray line can then be explained by either t-channel or s-channel annihilation

processes [4]. The former process necessarily involves an electrically charged particle, taken as a fermion below. Without loss of generality, the s-channel case assumes the presence of an intermediate gauge boson, which we shall take as leptophilic.

A. Heavy fermion mediator F

In the first model that we consider, the scalar DM particle, denoted by ϕ, couples to the SM via heavy fermionic mediators. For the sake of generality, we take ϕ to be complex but mention applicable formulas for real ϕ along the way. Concretely, ϕ and its antiparticle ϕ^* may couple to the SM charged and neutral leptons $l = (l_L^-, l_R^-)^T$ and ν_l through a Yukawa-like interaction with the introduction of new electrically charged and neutral fermions $F^\pm$ and F^0, arranged as part of an SU(2)$_L$ doublet (F_L^0, F_L^-), as well as singlets F_R^0 and F_R^-. Written in terms of Dirac fields $F = (F_L^-, F_R^-)^T$ and $F^0 = (F_L^0, F_R^0)^T$, the Lagrangian reads

$$\mathcal{L}_F = -c_L^l \phi \bar{F} P_L l - c_R^l \phi \bar{F} P_R l - c_L^l \phi \bar{F}^0 P_L \nu_l + \mathrm{H.c.} \qquad (2)$$

Here, (ν_l, l_L^-) and l_R^- are the SU(2)$_L$ doublets and singlets of lepton flavor $l = e$, μ, τ; $P_L = (1-\gamma^5)/2$ and $P_R = (1+\gamma^5)/2$ are the projection operators. We take all couplings to be real. In the presence of right-handed neutrinos ν_R, additional interactions become possible:

$$\mathcal{L}_F' = -c_R^l \phi (\bar{F}_R^0 \nu_R) + \mathrm{H.c.} \qquad (3)$$

For the purpose of this paper, we shall not consider the latter option in any detail but mention applicable results in passing.

There are a number of options related to Eq. (2); see, e.g., [44–50]. In what follows, we usually drop the superscript on $c_{L,R}^l$ for the coupling to electrons and electron neutrinos, as we consider them as always present, $c_{L,R} \equiv c_{L,R}^e$. Nonzero couplings to the second and third generations are *a priori* not the main focus of the paper, but they lead to further interesting consequences. Among them is a contribution to the anomalous magnetic moment of the muon, discussed below. If there is a single generation of heavy fermions F—which is the way the Lagrangian is written— one may additionally induce lepton-flavor-violating processes between the electron sector and muon or tau sector for $c^\mu \neq 0$ or $c^\tau \neq 0$, respectively (see below). At the expense of considering three generations of heavy fermions F_l, the flavor symmetry can be restored. Finally, we note that there is also a global dark U(1) or Z_2 symmetry in Eq. (2) between ϕ and F; the former (latter) applies for F^0 being Dirac (Majorana).

Because of collider bounds on charged particles [51], the fermions F have to be above the EW scale. Therefore, we take the advantage that they never appear on shell in any process considered here and derive constraints on the

effective UV-scale $\Lambda_F = (c_L c_R / m_F)^{-1}$. Before constraining the model, we infer the normalization points for the couplings from two particularly important predictions: the contribution to the anomalous magnetic lepton moment as well as the DM annihilation cross section corresponding to the INTEGRAL signal and the thermal relic.

1. Anomalous magnetic moment

Under the assumption that $m_F \gg m_\phi \geq m_l$ and that all c^l couplings are real, the one-loop contribution to the leptonic anomalous magnetic moment, shown in the left panel in Fig. 3, is given by

$$\Delta a_l^{(F)} = \frac{c_L^l c_R^l}{16\pi^2} \frac{m_l}{m_F}, \qquad (4)$$

in agreement with previous calculations [4,52]; note that $a_l \equiv (g_l - 2)/2$. Therefore, to address the long-standing muonic $g - 2$ anomaly [19]

$$a_\mu^{\mathrm{exp}} - a_\mu^{\mathrm{SM}} = (290 \pm 90) \times 10^{-11}, \qquad (5)$$

the corresponding favoured region is $c_F^\mu \equiv \sqrt{|c_L^\mu c_R^\mu|} \sim (5.5\text{–}7.6) \times 10^{-2}$ with $m_F = 1$ TeV. The full expression without assuming the mass hierarchy is given in Appendix A. In anticipation of the constraints to be derived below, we point out that the contribution (4) to the electron anomalous magnetic moment will be of central importance when assessing the viability of explaining various anomalies.

2. DM annihilation

In the model with heavy fermionic mediators $F^\pm$ and F^0, the nonrelativistic DM annihilation cross section into $e^+ e^-$ via $F^\pm$ exchange or into Dirac electron neutrinos via F^0 exchange with the participation of a (kinematically unsuppressed) light right-handed state given in Eq. (3), $\bar{\nu}_e \nu_R$ or $\bar{\nu}_R \nu_e$, reads

$$\sigma_{\mathrm{ann},F} v_M = \frac{c_L^2 c_R^2}{4\pi m_F^2} \left(1 - \frac{m_l^2}{m_\phi^2}\right)^{3/2} + \frac{3 c_L^2 c_R^2 m_l^2 v_{\mathrm{rel}}^2}{32\pi m_F^2 m_\phi^2} \sqrt{1 - \frac{m_l^2}{m_\phi^2}}, \qquad (6)$$

where $v_M = 2(1 - 4m_\phi^2/s)^{1/2}$ is the Møller velocity. The s-wave component agrees with the one in Eq. (1) in Ref. [4], while the p-wave component is different, due to the fact that we expand in the Lorentz-invariant product $\sigma_{\mathrm{ann},F} v_M$ rather than $\sigma_{\mathrm{ann},F} v_{\mathrm{rel}}$; see Appendix B 1 for the full expressions, as well as those for real scalar DM. Above, we have omitted terms that are suppressed by $(m_{l,\phi}/m_F)^4$ as well as higher-order terms. For the special case $c_L c_R = 0$ and for $m_l \to 0$, the above cross section vanishes, and the process becomes d-wave dominated [53–55], scaling as

$v_{\mathrm{rel}}^4 m_\phi^6 / m_F^8$. Given a TeV-scale F and $m_{l,\phi}$ well below GeV scale, the latter terms do not contribute to the annihilation cross section in any appreciable way. Finally, for real scalar ϕ, a factor of 4 should be multiplied to the expression in Eq. (6), as both t- and u-channel processes contribute.

The annihilation to a pair of left-handed neutrinos $\bar{\nu}_l \nu_l$, mediated by F^0, is either suppressed by neutrino mass or $1/m_F^4$ or v^2/m_F^4, for Dirac neutrinos; see Eqs. (B1) and (B2). However, if neutrinos are Majorana fermions, one may additionally annihilate to $\nu_l \nu_l$ or, equivalently, $\bar{\nu}_l \bar{\nu}_l$ with an s-wave cross section similar to Eq. (6) [56]. We comment on this possibility when considering cosmological constraints.

While we do not presume any production mechanism of the observed DM relic abundance, we will show the required parameters for thermal freeze-out below. Here, the DM abundance is $\Omega_\phi h^2 = 0.1198$ [57], where Ω_ϕ is the density parameter of ϕ and h is the Hubble constant in units of 100 km/s/Mpc. The observed relic density is achieved with $c_F^2 \sim 0.01\text{–}0.1$ for $m_\phi < \mathcal{O}(\mathrm{GeV})$ and $m_F \sim \mathcal{O}(100\ \mathrm{GeV})\text{–}\mathcal{O}(\mathrm{TeV})$ [4]. The parameter regions that yield the required annihilation cross section within uncertainties for both the thermal freeze-out and the INTEGRAL 511 keV line [18] are shown in Fig. 6 for $m_F \gg m_\phi$.

Although, as detailed in Sec. II, the 511 keV line prefers a DM mass below several to tens of MeV, we scan over the entire MeV–GeV mass range, as our results bear greater generality. In Figs. 6 and 7 below, we indicate by a lighter shading of the INTEGRAL favored bands the weakest constraint on m_ϕ that is derived from the INTEGRAL x-ray data themselves [42], $m_\phi \geq 70$ MeV.

B. Leptophilic vector mediator Z'

Turning now to the model with a gauge boson Z', both the DM particle ϕ and SM leptons are charged under the new U(1). The interactions have the form

$$\mathcal{L}_{Z'} = g_\phi^2 Z_\mu' Z'^\mu \phi^* \phi - i g_\phi Z_\mu' [\phi^* (\partial^\mu \phi) - (\partial^\mu \phi^*) \phi]$$
$$- Z_\mu' \bar{l} \gamma^\mu (g_L P_L + g_R P_R) l. \qquad (7)$$

The couplings $g_{L,R}$ and g_ϕ are understood as a product of gauge coupling g and charge assignments $q_{L,R}$ and q_ϕ so that $g_{L,R} = g q_{L,R}$ and $g_\phi = g q_\phi$, respectively. Again, there are many options available with Eq. (7). They generally differ by the Z' mass $m_{Z'}$, by their chiral couplings, by the absence or presence of family universality and/or kinetic mixing, by their (extended) Higgs sector, by potential additional fields that are required to cancel associated gauge anomalies in the UV, and so forth; see, e.g., [58] and references therein.

Here, we are primarily focused on the phenomenology associated with the Z' coupling to electrons and shall take g_L and g_R as flavor blind for when muons are involved. The special cases $g_l \equiv g_L = g_R$ and $g_L = -g_R$ correspond to a
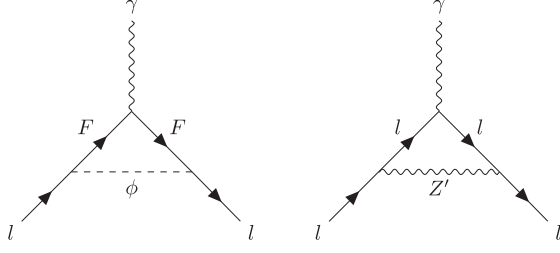
FIG. 3. Left: contribution to $(g-2)_l$ from ϕ and F particles. Right: contribution to $(g-2)_l$ from new Z' interaction.

pure vector and axial-vector interactions, respectively.[2] For the purpose of illustration, we consider $m_{Z'} \geq 10$ GeV in most of our discussions. As will be shown, only a Z' below the EW scale is of relevance for the INTEGRAL signal, so appears on shell at high-energy colliders. As a result, although Z' is generally off shell for the low-energy phenomenology, and bounds derived below can be represented using $\sqrt{g_\phi g_l}/m_{Z'}$, results from LEP need to be treated with caution. For the latter, we provide bounds both on $\sqrt{g_\phi g_l}/m_{Z'}$ in the heavy mediator limit and on $\sqrt{g_\phi g_l}$ for $m_{Z'} \ll m_Z$. The possibility of a Z' below 10 GeV will be discussed separately in Sec. VI.

1. Anomalous magnetic moment

Similarly as above, for the case $m_{Z'} \gg m_l$, the one-loop contribution to $(g-2)_l$ is given by

$$\Delta a_l^{(Z')} = \frac{6g_L g_R - 2(g_L^2 + g_R^2)}{24\pi^2} \frac{m_l^2}{m_{Z'}^2}, \qquad (8)$$

in agreement with Refs. [62,63] if a pure vector coupling $g_L = g_R \equiv g_l$ is assumed. The full expression of Eq. (8) is found in Appendix A. The associated diagram of interest is shown in the right panel in Fig. 3, and the $(g-2)_\mu$ favoured parameter space is $g_l/m_{Z'} \sim (4.6-6.4)$ TeV^{-1}. The constraint from $(g-2)_e$ will be evaluated in Sec. IV C.

For a flavor-blind g_l assumed here, the combination of several experiments excludes the possibility that this simple model explains the muonic $g-2$ anomaly. This conclusion holds irrespective of whether Z' decays dominantly into SM leptons or into DM particles, as the leading constraint comes from the measurements of electron-neutrino scattering [64].[3]

2. DM annihilation

For the annihilation cross section via a s-channel Z', the s-wave component vanishes, as scalars have no spin, and the p-wave component reads

$$\sigma_{\mathrm{ann},Z'} v_M = v_{\mathrm{rel}}^2 \frac{4m_\phi^2(g_L^2 + g_R^2) - m_l^2(g_L^2 - 6g_L g_R + g_R^2)}{48\pi(m_{Z'}^2 - 4m_\phi^2)^2}$$
$$\times g_\phi^2 \sqrt{1 - m_l^2/m_\phi^2}. \qquad (9)$$

It agrees with Eq. (3) in Ref. [4] when taking $v_{\mathrm{rel}} \simeq 2v_\phi$, where v_ϕ is the DM velocity. Since the cross section varies only by about a factor of 2 when either $g_R = 0$ or $g_L = 0$, we do not distinguish the left- and right-chiral couplings any further for annihilation and simply take $g_L = g_R \equiv g_l$ in the remainder. For real scalar DM, the annihilation would be extremely suppressed, since the Z' does not couple to a pair of real scalars at tree level.

Taking the DM annihilation $\phi\phi^* \to Z'^* \to l^- l^+$ with cross section as above, for $m_{Z'} \gg m_\phi > m_l$, the parameter region of interest for INTEGRAL is shown by the red and blue bands in Fig. 7 for NFW and Einasto profiles, respectively. Finally, we note that the observed DM relic abundance is achieved when [4]

$$g_\phi g_l \sim (3-12) \times \left(\frac{m_{Z'}}{10 \text{ GeV}}\right)^2 \left(\frac{m_\phi}{\text{MeV}}\right)^{-1}, \qquad (10)$$

in the limit of $m_{Z'} \gg m_\phi$. Obviously, $m_{Z'}$ around or above the EW scale puts us into the nonperturbative regimes and is not of interest for us. Depending on the Z' decay width, resonant annihilation at the point $m_{Z'} \simeq 2m_\phi$ introduces additional velocity dependence in the annihilation. A detailed investigation of the resonant point, such as performed in Refs. [26,66,67], is beyond the scope of this paper. Because of these reasons, we focus on $m_{Z'} \geq 2.1m_\phi$.

IV. LABORATORY CONSTRAINTS

The dark sector particles may be produced in the laboratory, especially at electron-beam facilities, through electron-positron annihilation in colliders (Fig. 4) or electron-nuclei bremsstrahlung in fixed-target experiments (Fig. 5). Moreover, they can also appear virtually through loops, affecting EW precision measurements. Such considerations thus put upper bounds on the coupling of SM particles to the dark sector.

We briefly introduce the experimental data of interest and our methods to derive the related constraints below and

---

[2]For GeV fermionic DM with a leptophilic Z', see, e.g., [59–61].

[3]Other Z' options such as U(1)$_{L_\mu - L_\tau}$ remain allowed for resolving $(g-2)_\mu$, as most recently illustrated in Ref. [65]. For bounds on other relevant DM models, see, e.g., [63].
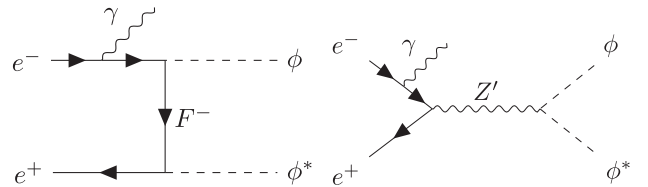

FIG. 4. Pair production of ϕ in electron-positron annihilation in association with initial state radiation. Photon emission from the intermediate charged F is suppressed and, hence, neglected.
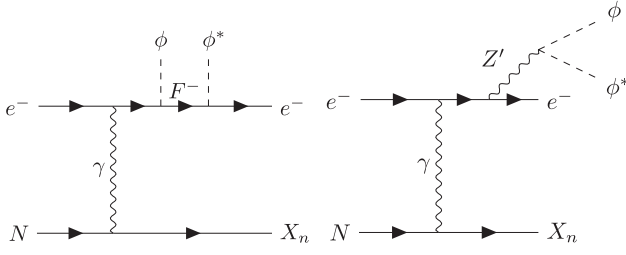
FIG. 5. Pair production of ϕ in electron-beam fixed-target experiments. We consider ϕ emission from both initial and final state electrons (but not from the heavy F particle). Note that a global dark symmetry in Eq. (2) forbids the diagram with ϕ and ϕ^* interchanged for the left process; see the main text.

refer to Ref. [68] and our Appendixes for further details of relevant cross sections.

A. Electron-beam facilities

We first consider intensity-frontier experiments, including low-energy electron-positron colliders and electron-beam fixed-target experiments. For the values of m_F and $m_{Z'}$ concerned above, we can produce ϕ only via off-shell mediators in these experiments.

Following our previous work [68], we derive the expected number of signal events and constraints from current experiments such as *BABAR* [69], NA64 [70,71], and mQ [72,73], as well as projected sensitivities for future ones, including Belle II [74,75], LDMX [76], and BDX [77]. Depending on the observable signatures, these experiments can be put in three categories described below.

The first category is to look for large missing transverse momentum or energy, accompanied by a monophoton signal, in low-energy electron-positron colliders, such as *BABAR* and Belle II. The expected number of signal events in each energy bin reads

$$N_{\rm sig}^{(i)} = \epsilon_{\rm eff} \mathcal{L} \int_{{\rm bin},i} \frac{ds_{\phi\phi}}{s} \int_{\cos\theta_\gamma^{\min}}^{\cos\theta_\gamma^{\max}} d\cos\theta_\gamma \frac{d\sigma_{e^-e^+\to\phi\phi\gamma}}{dx_\gamma d\cos\theta_\gamma}, \quad (11)$$

where $\epsilon_{\rm eff}$ is the efficiency, $\mathcal{L}$ is the integrated luminosity, $\theta_\gamma^{\max,\min}$ are the cuts on the photon angle in center-of-mass (c.m.) frame with respect to the beam axis, $x_\gamma = E_\gamma/\sqrt{s}$ is the energy fraction carried away by the photon with s, and $s_{\phi\phi} = (1 - x_\gamma)s$ is the c.m. energy square of e^-e^+ and ϕ pair, respectively. The differential cross section is found in Appendix B 2. For *BABAR*, we take the data of the analysis of monophoton events in a search for invisible decays of a light scalar at the $\Upsilon(3S)$ resonance [69]. The c.m. energy is 10.35 GeV, with two search regions of 3.2 GeV $\leq E_\gamma \leq$ 5.5 GeV and 2.2 GeV $\leq E_\gamma \leq$ 3.7 GeV.[4] For Belle II, we

---

[4]We do not consider possible resonant conversion of $\Upsilon(3S) \to Z'$ plus a low-energy photon, as $m_{Z'} = 10$ GeV is chosen arbitrarily.

follow Ref. [78] and derive the projection by scaling up the *BABAR* background to an integrated luminosity of 50 ab^{-1} with a similar c.m. energy.

The second category describes the missing energy search in electron-beam fixed-target experiments, such as NA64 and future LDMX. The expected number of signal single-electron events is given by

$$N_{\rm sig} = N_{\rm EOT} \frac{\rho_{\rm target}}{m_N} X_0 \int_{E_{\min}}^{E_{\max}} dE_3 \epsilon_{\rm eff}(E_3)$$
$$\times \int_{\cos\theta_3^{\min}}^{\cos\theta_3^{\max}} d\cos\theta_3 \frac{d\sigma_{2\to4}}{dE_3 d\cos\theta_3} \quad (12)$$

in the thin target limit, where $N_{\rm EOT}$ is the number of electrons on target (EOT), $\rho_{\rm target}$ is the mass density of the target, m_N is the target nuclei mass, X_0 is the radiation length of the target, E_3 is the energy of the final state electron, and θ_3 is the scattering angle with respect to the beam axis of the final state electron in the lab frame, with its detection efficiency given by $\epsilon_{\rm eff}(E_3)$. The differential cross section is derived in Appendix B 3. The background in such experiments is usually negligible after imposing stringent selection criteria. The NA64 experiment uses an electron beam with $E_{\rm beam} = 100$ GeV and has collected data of $N_{\rm EOT} = 4.3 \times 10^{10}$. We select events with only a final state electron, with its energy between $[0.3, 50]$ GeV and $\theta_3 \leq 0.23$ rad. For the proposed LDMX experiment, we use the benchmark values of phase I with $N_{\rm EOT} = 4 \times 10^{14}$ at $E_{\rm beam} = 4$ GeV and phase II with $N_{\rm EOT} = 3.2 \times 10^{15}$ at $E_{\rm beam} = 8$ GeV. The energy and geometry cuts on final state electrons are 50 MeV $< E_3 < 0.5 E_{\rm beam}$ and $\theta_3 < \pi/4$. A constant $\epsilon_{\rm eff} = 0.5$ is taken for both experiments.

The last category includes mQ and BDX, which are electron-beam fixed-target experiments designed to directly observe $\phi - e$ (or ϕ-nucleon) recoil events in a downstream detector. The expected number of electron recoil events is given by

$$N_{\rm sig} = n_e L_{\rm det} \int_{m_\phi}^{E_\phi^{\max}} \int_{E_R^{\rm th}}^{E_R^{\max}} dE_R \epsilon_{\rm eff}(E_R) \frac{dN_\phi}{dE_\phi} \frac{d\sigma_{\phi-e}}{dE_R}, \quad (13)$$

where n_e is the electron number density in the detector and $L_{\rm det}$ is the detector depth. The threshold recoil energy $E_R^{\rm th}$ depends on the experiment, and $E_R^{\max}$ reads

$$E_R^{\max} = \frac{2m_e(E_\phi^2 - m_\phi^2)}{m_e(2E_\phi + m_e) + m_\phi^2}, \quad (14)$$

with the exact differential recoil cross section given in Appendix B 4. The production spectrum of ϕ is computed by

$$\frac{dN_\phi}{dE_\phi} = 2N_{\rm EOT} \frac{\rho_{\rm target}}{m_N} X_0 \int_{E_\phi}^{E_{\rm beam}} dE$$
$$\times \int_{\cos\theta_\phi^{\rm min}}^{\cos\theta_\phi^{\rm max}} d\cos\theta_\phi I(E) \frac{d\sigma_{2\to4}}{dE_\phi d\cos\theta_\phi}, \quad (15)$$

in which the factor 2 accounts for the production of the ϕ pair, θ_ϕ is the scattering angle with respect to the beam axis of the produced ϕ in the lab frame with boundaries given by the geometry of the downstream detector, and $I(E)$ is the integrated energy distribution of electrons during their propagation in the target [68]. The differential cross section for the ϕ energy distribution is listed in Appendix B 3. For the mQ experiment, the incoming electron with energy $E_{\rm beam} = 29.5$ GeV impinges upon a tungsten target with $N_{\rm EOT} = 8.4 \times 10^{18}$. The Collaboration has reported 207 recoil events above the background, which is below the uncertainty of the latter $\sigma_{\rm bkg} = 382$ within the signal time window. We derive the upper bounds on the dark sector couplings from events with electron recoil energy $E_R \geq 0.1$ MeV. For BDX, electrons with $E_{\rm beam} = 11$ GeV are incident on an aluminum target, which comprises 80 layers with a thickness of 1–2 cm each. The BDX Collaboration estimated that for $N_{\rm EOT} = 10^{22}$ the number of background events with $E_R \geq 0.35$ GeV is about 4.7 [79]. Again, we consider only electron recoil events, with a detection efficiency of 100% for mQ [73] and 20% for BDX [79].

B. High-energy colliders

High-energy colliders may produce any of the dark sector particles studied here, leading to missing energy signatures. In the F model, a TeV-mass charged fermion F remains largely unconstrained by current bounds from LEP or LHC data, while the missing energy search in LEP [80] is able to constrain the overall coupling as

$$c_F^2/m_F \lesssim 1.23 \text{ TeV}^{-1}, \quad (16)$$

which can be improved by investigating DM production via Drell-Yan processes with high-luminosity LHC [48], as well with International Linear Collider [81].

For the Z' model, the LEP bound varies depending on the Z' mass. For a heavy Z' above the LEP energy scale, we obtain a bound from missing energy events induced by DM pair production as

$$\sqrt{g_\phi g_l}/m_{Z'} \lesssim 2.89 \text{ TeV}^{-1}, \quad (17)$$

in agreement with previous results [82,83], which is stronger than the reach of low-energy beam experiments. Although this is shown in Fig. 7, it does not apply to $m_{Z'}$ below the LEP energy scale, where a more proper LEP bound may come from missing energy induced by on-shell Z' production, requiring $g_l \lesssim 0.01$ [84]. Its combination with the perturbative condition $g_\phi^2/(4\pi) \lesssim 10$ results in

$$\sqrt{g_\phi g_l} \lesssim 0.335, \quad (18)$$

being comparable to the *BABAR* bound for $m_{Z'} = 10$ GeV. Naively speaking, these two LEP bounds, valid for different parameter regions of $m_{Z'}$, converge at $m_{Z'} \sim m_Z$. Projected sensitivities on a leptophilic Z' portal have also been derived for future colliders; see [61,85–88].

C. Precision observables induced by loops

The measurement of the fine structure constant α has been improved significantly with Cs atom interferometers [32]. Taking as input $\alpha \equiv \alpha^{\rm (Cs)}$, the SM prediction of the electron anomalous magnetic moment $a_e^{\rm (Cs)} = a_e^{\rm SM}(\alpha^{\rm (Cs)})$ is now in 2.5 σ tension with the direct measurement of a_e [89], $a_e^{\rm (meas)} - a_e^{\rm (Cs)} = -0.88(0.36) \times 10^{-12}$. At face value, this puts a stringent requirement on a new physics contribution:

$$\Delta a_e^{\rm BSM}|_{\rm Cs} \in (-0.88 \pm 3 \times 0.36) \times 10^{-12}$$
$$= [-1.96, 0.20] \times 10^{-12} \quad (19)$$

with a nominal 3σ requirement. Most recently, another experiment, using the recoil velocity on a Rb atom, has measured the value of the fine-structure constant with similar uncertainty [33]. Its value of α suggests a smaller a_e, in better agreement with the direct measurement, $a_e^{\rm (meas)} - a_e^{\rm (Rb)} = 0.48(0.30) \times 10^{-12}$. From this, we can obtain a similar constraint on the new physics contribution:

$$\Delta a_e^{\rm BSM}|_{\rm Rb} \in [-0.42, 1.38] \times 10^{-12}. \quad (20)$$

These differences above could also be rephrased in tensions between α extracted from Cs and Rb experiments and from direct a_e measurements using the standard model prediction $\alpha(a_e^{\rm SM})$, i.e., in $\alpha^{\rm (Cs/Rb)} - \alpha(a_e^{\rm SM})$. Both models—through their contribution to a_e—then imply an inferred shift in the value of α. One should obtain the same constraints from both.

In the F model, positive (negative) $c_L c_R$ yields a positive (negative) contribution; cf. Eq. (4) or the full expression in Appendix A. As shown in Fig. 6, either sign then puts a strong constraint on the model with a F mediator. In the Z' model, $g_L = g_R$ and $g_L = -g_R$ can also give a distinct contribution to a_e; see Eq. (8). A conservative limit can be given by combining the weaker of each limits of Eqs. (19) and (20), i.e., the lower bound from $\Delta a_e^{\rm BSM}|_{\rm Cs}$ and the upper bound from $\Delta a_e^{\rm BSM}|_{\rm Rb}$. This yields

$$4.3 \times 10^{-4} \text{ TeV}^{-1} \geq c_L c_R/m_F \geq -6.1 \times 10^{-4} \text{ TeV}^{-1},$$
$$625 \text{ TeV}^{-2} \geq g_L g_R/m_{Z'}^2 \geq -178 \text{ TeV}^{-2},$$

for the F and Z' model. In contrast, the combination of the stronger limits results in
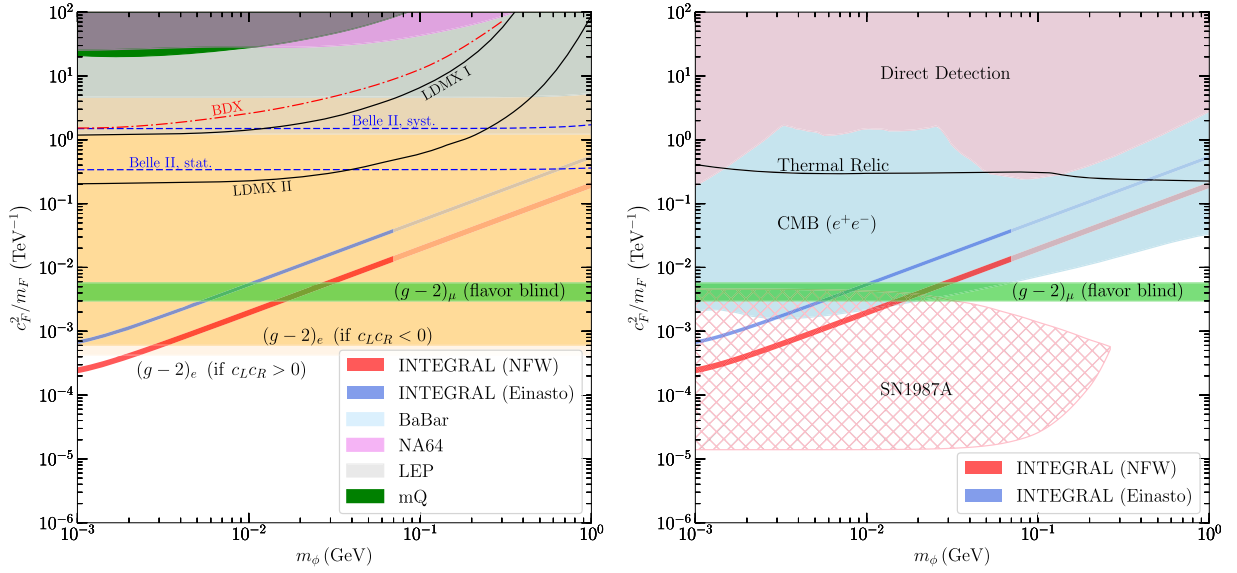
FIG. 6. Bounds on the inverse of effective UV-scale $\Lambda_F^{-1} = c_F^2/m_F$ in the F-mediated model from laboratory experiments (left) and from astrophysical observations including direct detection (right). The parameter regions of interest for the INTEGRAL excess are shown as thin blue and red bands; for $m_\phi \geq 70$ MeV, the DM interpretation is disfavored from INTEGRAL itself [42] as indicated by a lighter shading. The green horizontal band where $(g-2)_\mu$ is explained carries the assumption $c_F^\mu = c_F^e$. The $(g-2)_e$ constraint is the conservative one based on Refs. [32,33], for both $c_L^e c_R^e < 0$ and $c_L^e c_R^e > 0$.

$$6.2 \times 10^{-5} \text{ TeV}^{-1} \geq c_L c_R/m_F \geq -1.3 \times 10^{-4} \text{ TeV}^{-1},$$

$$91 \text{ TeV}^{-2} \geq g_L g_R/m_{Z'}^2 \geq -38 \text{ TeV}^{-2}.$$

For the Z' model, the $(g-2)_e$ constraint is always surpassed by the LEP bound above, for both $m_{Z'} \gg m_Z$ and $m_{Z'} \leq m_Z$, and is hence not included in Fig. 7; see Fig. 2.[5]

One may exercise some caution if exclusively applying Eq. (19), as it takes a positive half-σ shift to rule out any model by increasing the 2.5σ tension to 3σ. Here we stress that both the F- and Z'-mediated models allow for both signs in their contributions. Therefore, going in the other direction, one may first bring both measurements into reconciliation and, in a further consequence, allow for a particularly large shift before the lower boundary in Eq. (19) is reached. In this sense, Eq. (19) entails both an aggressive and a conservative limit. In Fig. 6, we show the conservative limits that arise from the combination of Eqs. (19) and (20).

The invisible decay $Z \to \phi\phi^*$ induced by the one-loop diagram containing F or Z' will alter the decay width of Z; see Fig. 9. Such an additional contribution is bounded by experiments [91] to satisfy

$$\Gamma(Z \to \text{inv})_{\text{new}} \lesssim 0.56 \text{ MeV} \quad \text{at 95\% C.L..} \quad (21)$$

Explicit calculation of the relevant loop diagrams, detailed in Appendix C, reveals that the ensuing constraints ($c_F/m_F < 26.6$ TeV^{-1} and $\sqrt{g_\phi g_l} < 0.35$ for $m_{Z'} = 10$ GeV) are weaker than those above from general missing energy searches. We hence do not show this constraint in the figures.

D. Further precision tests

Before closing this section, we also mention that further limits arise when the models introduce new sources of parity or flavor violation.

The effect of parity violation can be parametrized as a deviation from the SM-predicted value of the weak angle θ_W.[6] The E158 experiment at SLAC used polarized electron beams of $E_e \simeq 46$–48 GeV and measured the Møller scattering asymmetry with one polarized electron:

$$A_{\text{LR}} = \frac{d\sigma_{e_R e} - d\sigma_{e_L e}}{d\sigma_{e_R e} + d\sigma_{e_L e}} \quad (22)$$

at low momentum transfer $Q^2 \simeq 0.026$ GeV^2 [95,96]. The subtracted value of $4\sin^2\theta_W - 1$ from the data is $-0.0369(52)$, slightly higher than the SM prediction, $-0.0435(9)$ at low energy. For the Z' model with

---

[5]Another observable is the running of the fine structure constant, given by the photon vacuum polarization induced by the charged F loop, $\Pi(-M_Z^2) - \Pi(0)$. This number needs to be below 0.00018 [90], requiring $m_F \gtrsim 80$ GeV. The formula for $\Pi(p^2)$ is given in Eq. (C7) with g_l replaced by e. A dark U(1) gauge boson Z' does not contribute to the running at one loop.

[6]Here we note that there is no sensitivity from the feats that detected atomic parity violation [92] because of the leptophilic nature of couplings involved; see [93,94] for when a Z' coupling to quarks is present.
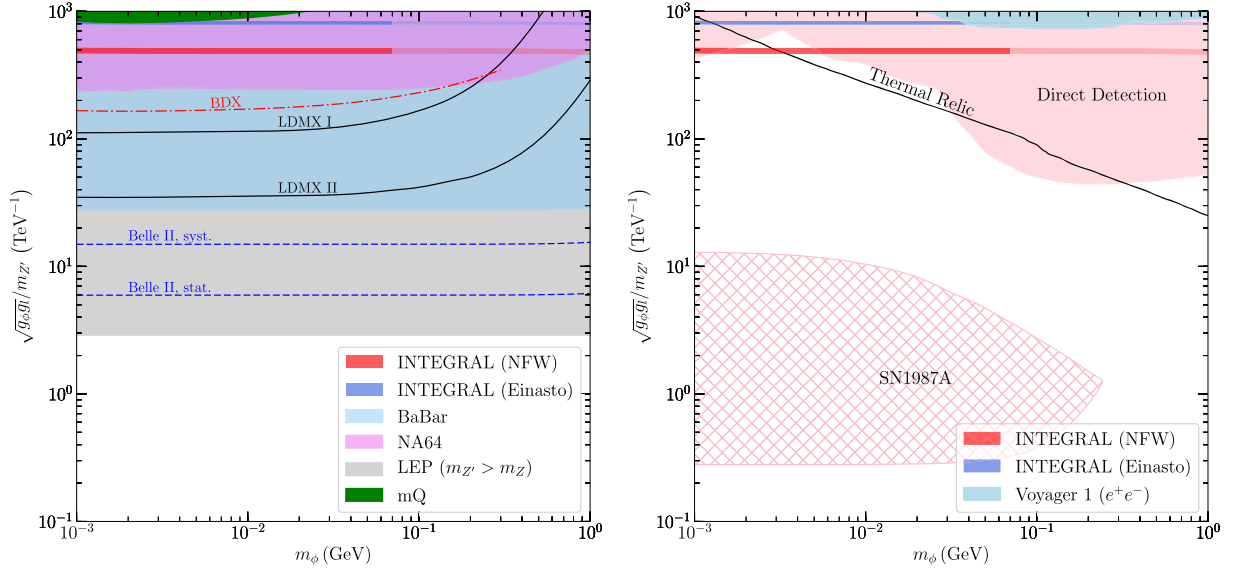
FIG. 7.   Bounds on the inverse of effective UV scale $\Lambda_{Z'}^{-1} = \sqrt{g_\phi g_l}/m_{Z'}$ for the Z' model from laboratory tests (left) and from cosmological and astrophysical probes including direct detection (right). The parameter regions of interest for the INTEGRAL excess are shown as thin blue and red bands; for $m_\phi \geq 70$ MeV, the DM interpretation is disfavored as indicated by a lighter shading. LEP bound applies only for $m_{Z'}$ above the EW scale, below which Eq. (18) applies instead. We do not show a band for $(g-2)_\mu$, which would need an assumption on g_ϕ/g_l, since it is already excluded elsewhere (see the main text and Fig. 2).

$m_{Z'} \gg \sqrt{Q^2}$, the resulting bound scales as $g_{R(L)}/m_{Z'} \lesssim$ 0.38(0.58) TeV^{-1} at $g_{L(R)} = 0$ and almost vanishes at $g_L = \pm g_R$. Moreover, at $g_L = g_R \cos 2\theta_W/(\cos 2\theta_W - 1)$, the contribution of Z' can be absorbed by rescaling the Fermi constant. Although for $m_{Z'} \geq 10$ GeV concerned in this section, it is at most comparable with the LEP bound above, future experiments, such as MOLLER [97] and P2 at MESA [98], have the potential to improve the limit by more than one order of magnitude [99,100]. In contrast, the F model does not induce additional electron scattering processes at tree level and, thus, can hardly be constrained by such experiments.

Moreover, if only one generation of F is present, nonzero couplings to the muon and tau sector induce lepton flavor violation, similar to flavored DM [44]. For example, one may have the decay $\mu \to e\gamma$ by closing the ϕ loop, effectively via the magnetic dipole interaction [101]. The current strongest limit, from the MEG experiment [102], requires $\mathrm{Br}_{\mu \to e\gamma} \lesssim 4.2 \times 10^{-13}$. This, in turn, gives $c_F^\mu c_F^e/m_F \lesssim 2.7 \times 10^{-5}$ TeV^{-1} if $c_L^l = c_R^l$ with $c_F^l \equiv \sqrt{|c_L^l c_R^l|}$. For purely chiral interaction with $c_L^l = 0$, the bound is relaxed to $\sqrt{|c_R^\mu c_R^e|}/m_F \lesssim 0.05$ TeV^{-1} as an additional spin flip is needed [103]; the same bound applies if one switches the chirality subscripts.

Another example is the decay $\mu \to e\phi\phi$ at a rate compared to the SM mode:

$$\frac{\Gamma_{e\phi\phi}}{\Gamma_{e\bar{\nu}_e\nu_\mu}} \sim \frac{m_W^4}{m_\mu^2 m_F^2} \quad \text{or} \quad \frac{m_W^4}{m_F^4}. \tag{23}$$

The first scaling applies for $(c_L^\mu c_R^e)^2 + (c_R^\mu c_L^e)^2 \neq 0$; the second scaling applies for when the same combination of couplings vanishes. Hence, because of the coupling structure and because of kinematic effects, one generally expects distortions of the electron spectrum. The latter is an important test for the $V - A$ nature of weak interactions and has been mapped out well in the coefficients describing it [91,104]. The sensitivity is, however, likely superseded by the radiative decay above and applies only to $m_\phi \leq m_\mu/2$; a detailed study of it is beyond the scope of this paper.

Finally, we mention that, for a Z' boson that couples to quarks or leptons with appreciable strength, precision observables were also investigated in Refs. [105,106]; note, however, that stringent constraints from dilepton resonance searches derived in the latter work are avoided, as in our setup Z' dominantly decays into a ϕ pair.

V. COSMOLOGICAL AND ASTROPHYSICAL CONSTRAINTS

As the scalar ϕ is assumed to be the dominant DM component, the models are also constrained by astrophysical and cosmological observables, as well as from DM direct detection experiments. These constraints are discussed in the following.

A. BBN and CMB ΔN_{eff} bounds

Here we take into account the big bang nucleosynthesis (BBN) and CMB bounds on N_{eff} from early Universe observations while at the same time remaining agnostic about the state of the Universe for $T \gtrsim$ MeV. Since

$m_\phi \sim \mathcal{O}(\text{MeV})$, during BBN ϕ can still be relativistic and contribute to the radiation density, summarized in the parameter N_{eff}. Recall that we always set $m_{Z'} \geq 2.1 m_\phi$, so Z' plays only a subleading role in the radiation density budget, even though it has three degrees of freedom. Currently, two relativistic degrees of freedom, like from a thermal complex scalar, are still considered to be marginally allowed by BBN on ΔN_{eff} [107–109].

In contrast, the Planck measurement of the CMB spectrum requires that $N_{\text{eff}} = 2.99 \pm 0.33$ at the last scattering surface [57]. This limits the residual DM annihilation after neutrino decoupling that injects energy either into the visible or into the neutrino sector [110,111]. In the F model, ϕ pairs annihilate into electrons. Under the assumption of a sudden neutrino decoupling at 1.41 MeV [112], we obtain a lower bound from N_{eff} as $m_\phi \geq 5.1$ MeV for a complex scalar, consistent with previous results [18].[7] However, the CMB bounds from N_{eff} become much weaker if the scalar DM annihilates into both electrons and neutrinos, which happens in the F model with Majorana neutrinos as well as in the Z' model. The underlying reason is that both the photon and neutrino fluid is being heated so that the ensuing offset in the ratio of their respective temperatures is milder; see, e.g., [113–115] for recent discussions. In a flavor-blind setup assuming DM annihilates to electrons and each species of SM neutrinos equally, we then estimate that the Planck bound on N_{eff} requires only $m_\phi \gtrsim 2.0$ MeV. The latter possibility was not considered in Ref. [18].

B. Direct detection

As we focus on sub-GeV mass ϕ particles, we consider the $\phi - e$ scattering signal, as it has a lower threshold on DM mass in direct detection experiments. Exclusion limits are customarily presented in terms of a reference scattering cross section [116]:

$$\bar{\sigma}_e = \frac{1}{16\pi(m_e + m_\phi)^2} \overline{|\mathcal{M}_{\phi-e}(q)|^2}_{q^2 = \alpha^2 m_e^2}, \qquad (24)$$

where $\overline{|\mathcal{M}_{\phi-e}(q)|^2}_{q^2 = \alpha^2 m_e^2}$ is the squared matrix element of ϕ scattering on a free electron, summed over final state spins and averaged over initial state spin, evaluated at a typical atomic momentum transfer $q = \alpha m_e$. To the order of $\mathcal{O}(v_{\text{rel}}^2)$, it is given by

$$\overline{|\mathcal{M}_{\phi-e}(q)|^2}_F = \frac{16 c_L^2 c_R^2 m_e^2}{m_F^2},$$

$$\overline{|\mathcal{M}_{\phi-e}(q)|^2}_{Z'} = \frac{16 g_\phi^2 g_l^2 m_\phi^2 m_e^2}{m_{Z'}^4}, \qquad (25)$$

---

[7]In the case of Dirac SM neutrinos with a kinematically accessible right-handed neutrino (as alluded to when introducing the models), one also would need to verify that ν_R decouples early enough from the thermal bath, so that, overall, the upper bound on N_{eff} is satisfied.

for the two representative models. Note that bounds on $\bar{\sigma}_e$ have been obtained for the present case of constant DM form factors, most recently in SENSEI [117], which also summarizes previous bounds from XENON10 [118,119] and XENON1T [120], as well as from considering a solar-reflected DM flux [121]. The corresponding constraints, combining the results of experiments mentioned above, are shown in Figs. 6 and 7.

C. Indirect search

To explain the INTEGRAL signal, ϕ has to be a symmetric DM candidate, implying ϕ annihilation into SM leptons both at epochs of BBN and CMB as well as at low redshift. Among them, bounds from BBN observables and DM annihilating to neutrinos [114,122] are very weak and are not further considered. Since in the considered models ϕ does not annihilate into photons at tree level (except when accompanied by final state radiation), we focus on the channel $\phi\phi^* \to e^+ e^-$.

For the F-mediated case, in which both s-wave and p-wave annihilation are present (6), it turns out that the constraint from CMB [123] is, in general, stronger than that from *Voyager 1* data [124]. In the Z'-mediated case, since the leading contribution of $\phi\phi^* \to e^+ e^-$ is p wave (9), the annihilation at CMB epoch is velocity suppressed and the bounds from present-day data such as from *Voyager 1* [39,125] is more stringent, disfavoring DM masses above $\mathcal{O}(30)$ MeV to explain the INTEGRAL 511 keV line. This will be further improved by about one order of magnitude in future experiments, such as e-ASTROGAM [43,126] and AMEGO [127]. The CMB constraint for the F case and the *Voyager 1* constraint for the Z' case are shown in Figs. 6 and 7, respectively.

D. Structure formation

To avoid the collisional damping of DM primordial fluctuations [128,129], DM has to kinetically decouple from the observable sector in the early Universe. In the considered models, DM couples to electrons and neutrinos with similar strength. Since the number density of electrons is much lower than that of background neutrinos once $T \ll m_e$, the scattering on neutrinos, hence, governs the ensuing constraint. Here we take the bounds derived in Refs. [130,131] for both energy-independent and energy-dependent DM-neutrino scattering cross sections. Concretely, we require that for the F model

$$\sigma_{\phi-\nu} \simeq \frac{c_F^4}{8\pi m_F^2} \lesssim 10^{-36} \left(\frac{m_\phi}{\text{MeV}}\right) \text{cm}^2 \qquad (26)$$

and for the Z' model

$$\sigma_{\phi-\nu} \simeq \frac{E_\nu^2 g_\phi^2 g_l^2}{2\pi m_{Z'}^4} \lesssim 10^{-41} \left(\frac{m_\phi}{\text{MeV}}\right) \left(\frac{E_\nu}{\text{eV}}\right)^2 \text{cm}^2. \quad (27)$$

The requirement consequently leads to $c_F^2/m_F \lesssim 0.25(m_\phi/\mathrm{MeV})^{1/2}\,\mathrm{TeV}^{-1}$, as well as $\sqrt{g_\phi g_l}/m_{Z'} \lesssim 2.17 \times 10^4 (m_\phi/\mathrm{MeV})^{1/4}\,\mathrm{TeV}^{-1}$. Both bounds are weaker than those obtained above and are not shown in the figures.

E. DM self-scattering

If ϕ constitutes DM, its self-interaction may change the shape and density profile of DM halos and the kinematics of colliding clusters. Such self-interaction is apparently very weak in the heavy F model.

In the Z' model, the DM particle ϕ can efficiently self-scatter via Z' exchange. The self-scattering cross section averaged over $\phi\phi \to \phi\phi$, $\phi\phi^* \to \phi\phi^*$, and $\phi^*\phi^* \to \phi^*\phi^*$ reads [132]

$$\sigma_{\mathrm{SI}}^{\phi\phi} = \frac{3g_\phi^4 m_\phi^2}{8\pi m_{Z'}^4}, \tag{28}$$

where velocity-suppressed terms have been neglected.[8] However, the current bound, $\sigma_{\mathrm{SI}}/m_\phi \leq 0.5\,\mathrm{cm}^2/\mathrm{g}$ from cluster observations [133–137], is also not able to provide any meaningful bounds on the Z' model with a 10 GeV $m_{Z'}$.

F. Anomalous supernova cooling

An important constraint arises from the anomalous energy loss via ϕ production in hot stars, especially inside supernovae (SN), as we consider $m_\phi = \mathcal{O}(\mathrm{MeV}\text{–}\mathrm{GeV})$ which has overlap with the SN core temperature. To avoid the suppression of neutrino emission from the SN core after explosion, we impose the so-called "Raffelt criterion," which states that the energy loss via dark particle production has to be smaller than the luminosity in neutrinos, $L_\nu = 3 \times 10^{52}\,\mathrm{erg/s}$ [138].[9] Here, we follow the method in Refs. [68,141,142] and adopt the SN1987A numerical model of Ref. [143] with a total size $r_{\mathrm{SN}} = 35$ km, to derive the bounds on the leptophilic DM models above.

The dominant ϕ production channel is pair creation from electron-positron annihilation. As our mediator particles F or Z' are much heavier than the core temperature of SN, we can safely neglect thermal corrections. Quantitatively, the lower boundaries of the exclusion regions are derived by requiring

$$\int_0^{r_c} d^3r \int \frac{d^3p_{e^-} d^3p_{e^+}}{(2\pi)^6} f_{e^-} f_{e^+} (\sigma_{e^-e^+ \to \phi\phi^*} v_M)\sqrt{s} \lesssim L_\nu, \tag{29}$$

where r_c is the core size of SN1987A, taken as 15 km here, and f_{e^-,e^+} are Fermi-Dirac distributions for electron and positron.

On the flip side, if the coupling between ϕ and SM particles inside the SN core is so strong that the ϕ becomes trapped inside the core, the energy loss via ϕ emission diminishes and again drops below the neutrino luminosity.[10] To estimate the corresponding upper boundaries of couplings, we first define a radius r_d, where a thermalized blackbody luminosity of ϕ equals L_ν [68,141]. Consequently, if ϕ gets further deflected by scattering off electrons for $r > r_d$, the effective dark luminosity drops below L_ν. In practice, we impose

$$\int_{r_d}^{r_{\mathrm{SN}}} dr \frac{1}{\lambda_{\phi-e}(r)} \leq 1. \tag{30}$$

Here, the mean-free path $\lambda_{\phi-e}$ at each radius is calculated by averaging the momentum distributions of both ϕ and electrons:

$$\lambda_{\phi-e}(r) = \frac{\langle n_\phi v_\phi \rangle}{\langle n_e n_\phi \sigma_{\phi-e} v_M \rangle}\bigg|_r, \tag{31}$$

where the Pauli blocking factor induced by final state electrons has been taken into account. The relevant differential cross sections are listed in Appendix B 4.

The resulting SN1987A exclusion regions, combining both lower and upper boundaries, are given in the right panels in Figs. 6 and 7. Our lower boundaries agree well with previous results [145,146]. Regarding the upper boundaries, we find that Pauli blocking plays an important role in suppressing ϕ-electron scattering. Meanwhile, although there is little Pauli blocking in ϕ-nucleon scattering, ϕ couples only to quarks at loop level, yielding a suppression by another factor m_ϕ^2/m_F^2 for the F model and α/π for the Z' model. It, hence, turns out that ϕ-electron scattering dominates the capture in the parameter regions studied here.

VI. Z' MASS BELOW 10 GeV

Now we consider $m_{Z'} \lesssim 10$ GeV, for which Z' may appear on shell in intensity-frontier experiments, c.m. energy permitting. In this case, the effective operator approach with its scale given by $\sqrt{g_\phi g_l}/m_{Z'}$ does not apply any longer. Nevertheless, the DM interpretation of the INTEGRAL signal relies only on the product $g_\phi g_l$, instead of on each of the two couplings individually, up to a

---

[8]At $m_{Z'} \sim 2m_\phi$ the velocity suppression in s-channel $\phi\phi^* \to \phi\phi^*$ can be compensated by the resonant enhancement. Such a resonant contribution never dominates and, thus, is not considered.

[9]The bounds from SN1987A are derived from the cooling of the protoneutron star; doubts exist if SN1987A was a neutrino-driven explosion [139], in which case the limits become invalidated. Such speculation could be resolved once the remnant of SN1987A is firmly observed [140].

[10]For even stronger couplings, the abundance of ϕ particles trapped inside SN may help to capture SM neutrinos, leading to an observable reduction in SN neutrino emission [144]. This may affect the parameter region studied in our Sec. VI for $m_\phi \lesssim 10$ MeV.
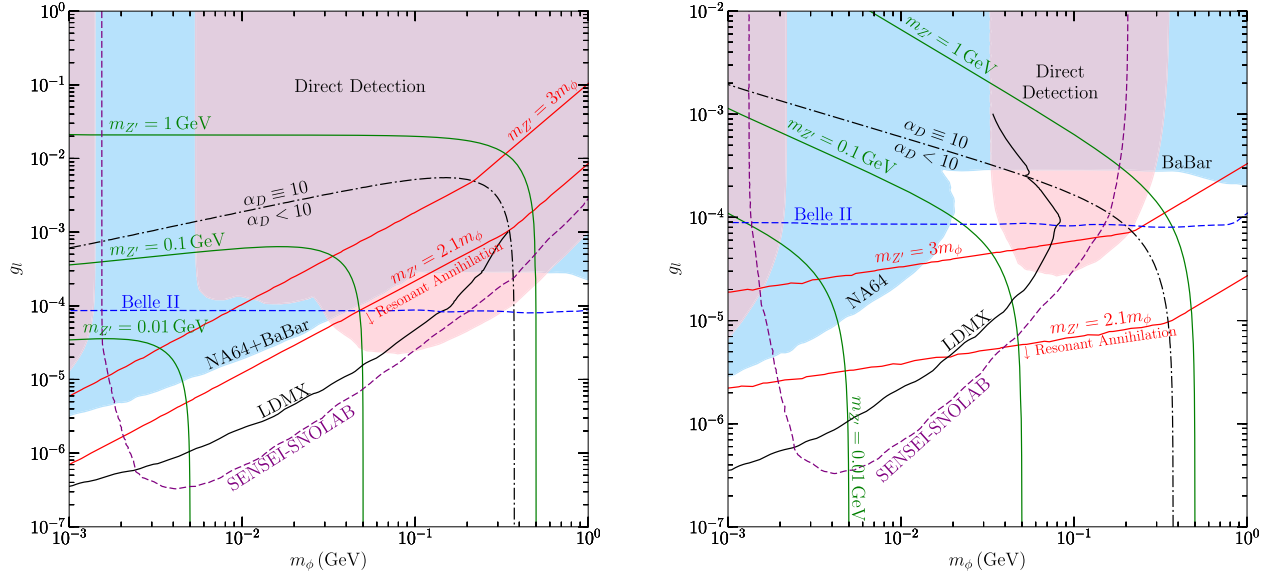
FIG. 8.   Conservative bounds on the lepton-Z' coupling g_l by saturating the cluster bound on the $\phi - Z'$ coupling g_ϕ and imposing either Eq. (1) for INTEGRAL (left) or successful thermal freeze-out (right) to fix $m_{Z'}$. Below the $m_{Z'} = 2.1 m_\phi$ line, DM annihilation happens resonantly at freeze-out or at low redshift. Additionally, Planck observations require $m_\phi \gtrsim 2$ MeV in the minimal setup.

minor effect of Z' decay width. Therefore, to obtain the most conservative constraints on g_l, we choose to maximize the dark coupling g_ϕ, using the cluster bounds [134,136,137] above:

$$\sigma_{\mathrm{SI}}/m_\phi \leq 0.5 \text{ cm}^2/\text{g}. \qquad (32)$$

We also impose a perturbativity bound, requiring that $\alpha_D = g_\phi^2/(4\pi)$ should not exceed 10.

There are then three parameters left. To explain the INTEGRAL signal, Eq. (1) allows one to solve for the value of $m_{Z'}$ for each choice of (m_ϕ, g_l). Now we directly adopt the existing constraints (e.g., NA64 and *BABAR*) and projected sensitivities (e.g., LDMX and Belle II) on an invisibly decaying Z' from Ref. [147]. For direct detection, we take the bounds with electron recoils summarized in Ref. [117] and future projections of SENSEI at SNOLAB in [148]. Interestingly, for m_ϕ below 100 MeV, this may be further improved by orders of magnitude using potential signals from neutron star heating [149–151]. Indirect bounds on p-wave DM annihilation are relatively weaker [114] and are not considered further.

The results are summarized in the left panel in Fig. 8. Below the dash-dotted line, a self-interaction cross section saturating Eq. (32) is achieved with $\alpha_D < 10$. Above the line, we set $\alpha_D = 10$ and the bound (32) is not saturated. Assuming smaller values of α_D necessarily requires larger values of g_l, while their product has to be large enough to explain the INTEGRAL signal. Therefore, this choice of α_D gives the most conservative bounds and choosing

smaller α_D would exclude more parameter space in Fig. 8. The green and red lines in the figure are the contours of $m_{Z'}$ and $m_{Z'}/m_\phi$, respectively. While $m_{Z'} = 3m_\phi$ has often been chosen in the literature, we also show the contour of $m_{Z'} = 2.1m_\phi$, below which the average DM kinetic energy may overcome the mass barrier to produce intermediate Z' on shell at freeze-out or after. As is shown in the figure, for each value of $m_{Z'}$ the mass ratio already becomes important in determining the annihilation cross section at $m_{Z'} = 3m_\phi$.

Our results suggest that most of the parameter region with nonresonant DM annihilation has been excluded, while the LDMX experiment is projected to probe the whole region of $m_{Z'} \gtrsim 2.1m_\phi$. This is different from the heavy $m_{Z'}$ case above, where Belle II always has a better sensitivity in probing the DM particle. In the presence of resonant annihilation, the required values of g_l can be much smaller than what fixed-target experiments will reach; thus, indirect DM searches, such as e-ASTROGAM [43], are expected to better probe this parameter region.

Similarly, instead of calibrating on INTEGRAL, we may alternatively fix the annihilation cross section by the thermal freeze-out requirement (right panel in Fig. 8). In this case, a limited parameter region is still allowed but will be probed by future fixed-target experiments, as well as future direct detection experiments using electron recoils. Our result is in agreement with previous studies which generally fix $m_{Z'} \equiv 3m_\phi$ and $\alpha_D = 0.1$ [147] (or 0.5 [152–154]) but have not considered dark matter self-interaction. For both panels in Fig. 8, the excluded region from Z' searches would reduce by choosing larger values of α_D. By

introducing the upper bound on α_D from Eq. (32), the exclusion in Fig. 8 is, hence, robust in both cases, i.e., either when imposing the DM interpretation of INTEGRAL (left) or when requiring successful thermal freeze-out (right).

VII. CONCLUSION

In this work, we consider the possibility that DM is a complex scalar particle ϕ with a mass below the GeV scale. The particle is assumed to couple to SM leptons, either via a charged fermion F or via a vector boson Z'. These models fare among the simplest UV-complete extensions to the SM and have been contemplated as sub-GeV DM candidates well before the field exploded with activity in this mass bracket. Among other reasons, they draw their attention from the fact that ϕ annihilation today might explain the galactic INTEGRAL excess and/or bring into reconciliation the prediction and observation of the anomalous magnetic moment of the muon.

Given the tremendous recent activity devoted to the search of light new physics, it is only timely to revisit these models of scalar DM in light of much new data. These particles can be probed in the laboratory, such as in electron-beam experiments, and by astrophysical and cosmological observations. We collate the latest observational and experimental data and subject the model to all relevant bounds and provide forecasts on the sensitivity of proposed future experiments.

Respecting the bounds on charged particles from high-energy colliders LEP and LHC, we consider F to be at or above the EW scale. The combination m_F/c_F^2 is inherent to most observables and can be interpreted as the effective UV-scale Λ_F for that model. We calculate the production of ϕ pairs, mediated by the exchange of off-shell F, in the fixed-target experiments NA64, mQ, LDMX, and BDX as well in e^+e^- colliders BABAR and Belle II. When the production is kinematically unsuppressed, the best bound is $\Lambda_F \gtrsim 250$ GeV by BABAR, currently surpassed by LEP with $\Lambda_F \gtrsim 1$ TeV. LDMX-II can improve on this number to 5 TeV. Turning to the Z' model, we consider both heavy and light vector mediators. If Z' remains off shell in all experiments, we may take the combination $m_{Z'}/\sqrt{g_\phi g_l}$ as the effective UV-scale $\Lambda_{Z'}$. In this case, BABAR points to $\Lambda_{Z'} \gtrsim 35$ GeV to be improved by Belle II to $\Lambda_{Z'} \gtrsim 170$ GeV at best, weaker than the current LEP bound of $\Lambda_{Z'} \gtrsim 346$ GeV.

These direct limits are then compared to loop-induced precision observables, concretely, to $g - 2$, to the invisible width of the Z, and to Z-boson oblique corrections. We explicitly revisit all those calculations, confirming previously presented scaling relations in the limit $m_{\phi,l}/m_F \ll 1$ or $m_{\phi,l}/m_{Z'} \ll 1$ and, as an added value, provide the full expressions of the loop integrals. We find that, for the F model, the improved limit obtained from $g - 2$ of the electron surpasses all direct observables, with

$\Lambda_F \gtrsim 10^4$ TeV, while, for the Z' model, they do not play a role in the phenomenology. We also complement those constraints with limits that arise from the freedom in the chiral structure of the models, using the parity asymmetry in polarized electron scattering. Finally, we derive limits from lepton flavor violation that are dependent on the concrete UV content of the models.

Turning to astrophysical constraints, we derive the anomalous energy loss induced by ϕ-pair production in the assumed protoneutron star of SN1987A. This adds strong and complementary new limits on the parameter space for $m_\phi \lesssim 100$ MeV down to $\Lambda_F \gtrsim 10^5$ TeV and $\Lambda_{Z'} \gtrsim 3$ TeV. We furthermore consider constraints from direct detection, structure formation, CMB energy injection, and DM self-scattering. Here, the CMB puts stringent constraints on the s-wave annihilation mediated by F. In turn, for the p-wave annihilation mediated by Z', the bounds are subleading. For those reasons, a thermal freeze-out in the F-mediated model is firmly excluded, whereas the Z' model remains little constrained from energy injection.

Regarding the DM interpretation of the INTEGRAL 511 keV line, we show that it is excluded in both the F-mediated model as well as in the Z'-mediated model with $m_{Z'} \geq 10$ GeV. In the model with charged F, the crucial constraints come from the $(g - 2)_e$ data, from the CMB, and from SN1987A. For the Z' model, intensity-frontier experiments and direct detection via electron recoils play the major role. However, a caveat exists: If the annihilation is resonant, $m_{Z'} \simeq 2m_\phi$, the INTEGRAL signal may still be explained in conjunction with a light $m_{Z'} \leq 10$ GeV while at the same time being experimentally allowed.

In a final part, we then entertain the possibility of a Z' mass below 10 GeV. The phenomenology then changes, as the vector may go on shell in various considered searches. To derive conservative constraints on the Z' coupling to the observable sector, g_l, we then saturate the dark coupling g_ϕ, taking its maximally allowed value from DM self-scattering. Requiring a successful explanation of INTEGRAL by fixing $m_{Z'}$ constrains the values of the remaining free parameters g_l and m_ϕ, driving m_ϕ to the resonant annihilation regime; the combination of LDMX, Belle II, and direct detection via electron recoils will be able to completely cover the parameter region of $m_{Z'} \geq 2.1m_\phi$ in the near future, i.e., the range where Z' remains off shell.

As an outlook, we comment on the resonant region which is not studied here. For $m_{Z'} \simeq 2m_\phi$, the annihilation cross section is greatly enhanced, and the required value on g_l coming from the annihilation cross section diminishes. This hampers the direct experimental sensitivity considered in this work. In turn, however, it opens the possibility of using displaced vertex searches in fixed-target experiments, depending on the decay mode of Z'. Dialing down the Z' mass further, $m_{Z'} < 2m_\phi$, the annihilation via $\phi\phi^* \to Z'^{(*)}Z'^{(*)} \to 2e^+2e^-$ will eventually come to dominate.

As the process is not velocity suppressed, we then reenter the regime where stringent CMB bounds apply. We leave those aspects to dedicated future work.

APPENDIX A: FULL EXPRESSION FOR $(g-2)_l$

From the explicit calculations for the $(g-2)_l$ contribution in the representative models as shown in Fig. 3, we obtain

$$\Delta a_l^{(F)} = \int_0^1 dz \frac{m_l(z-1)^2[m_l z(c_L^{l2}+c_R^{l2})+2c_L^l c_R^l m_F]}{16\pi^2[m_F^2(1-z)+m_\phi^2 z]},$$

$$\Delta a_l^{(Z')} = \int_0^1 dz \frac{m_l^2 z(z-1)[g_L^2(z+1)-4g_L g_R+g_R^2(z+1)]}{8\pi^2[m_l^2(z-1)^2+m_{Z'}^2 z]}.$$

$$(A1)$$

Taking only the leading-order terms and setting $g_L = g_R \equiv g_l$, we recover Eqs. (4) and (8) of the main text.

APPENDIX B: FORMULAS FOR CROSS SECTIONS

1. ϕ-pair annihilation

Here, we give the nonrelativistic expansion of the DM annihilation cross section via a t-channel fermion F, to second order of the relative velocity, assuming the hierarchy $m_F \gg m_\phi > m_l$:

$$\sigma_{\mathrm{ann},F} v_M = \frac{(c_L^2 m_l + c_R^2 m_l + 2c_L c_R m_F)^2}{16\pi(m_F^2+m_\phi^2-m_l^2)^2}\left(1-\frac{m_l^2}{m_\phi^2}\right)^{3/2} + v_{\mathrm{rel}}^2\left[\frac{(c_L^4-12c_L^2 c_R^2+c_R^4)m_\phi^2}{48\pi m_F^4}+\frac{3c_L^2 c_R^2 m_l^2}{32\pi m_F^2 m_\phi^2}-\frac{(c_L^4-14c_L^2 c_R^2+c_R^4)m_l^2}{64\pi m_F^4}\right].$$

$$(B1)$$

Here we have neglected terms of $O(m_{l,\phi}^5/m_F^5)$. By taking only the leading order in $O(m_{l,\phi}/m_F)$ and replacing v_{rel} with $2v_\phi$, we retrieve the s-wave expression of Eq. (1) in Ref. [4], while our p-wave result differs. The difference arises from the general mismatch between v_{rel} and v_M. We prefer to use the nonrelativistic expansion of the Lorentz-invariant quantity $\sigma_{\mathrm{ann}} v_M$ [157]; our scattering amplitude

agrees with the one given in the appendix of Ref. [4]. For the special case $c_L c_R = 0$ and for $m_l = 0$, the s-wave component in Eq. (B1) vanishes, and the process becomes p-wave dominated, scaling as $v_{\mathrm{rel}}^2 m_\phi^2/m_F^4$.

For real scalar DM, $\phi = \phi^*$, the annihilation process via a u-channel fermion F needs to be added, and the cross section in the same approximation becomes

$$\sigma_{\mathrm{ann},F}^{\mathrm{real}\phi} v_M = \frac{(c_L^2 m_l + c_R^2 m_l + 2c_L c_R m_F)^2}{4\pi(m_F^2+m_\phi^2-m_l^2)^2}\left(1-\frac{m_l^2}{m_\phi^2}\right)^{3/2} + v_{\mathrm{rel}}^2\left[\frac{3c_L^2 c_R^2 m_l^2}{8\pi m_F^2 m_\phi^2}+\frac{3c_L c_R(c_L^2+c_R^2)m_l^3}{8\pi m_F^3 m_\phi^2}-\frac{c_L^2 c_R^2 m_\phi^2}{\pi m_F^4}+\frac{3c_L^2 c_R^2 m_l^2}{4\pi m_F^4}\right].$$

$$(B2)$$

2. $e^- e^+$ annihilation with initial state radiation

First, we detail the annihilation cross section associated with initial state radiation (ISR), corresponding to Fig. 4. Following Ref. [68], the differential cross section with ISR is formulated as the cross section without ISR times the improved Altarelli-Parisi radiator function. The annihilation cross sections, without ISR and with s denoting the squared c.m. energy, to the order of $O(m_{e,\phi}^3/m_F^3)$ and after an average over the initial state spins has been performed, read

$$\sigma_{e^- e^+ \to \phi\phi}^{(F)} = \frac{c_L^2 c_R^2}{32\pi m_F^2}\sqrt{\frac{s-4m_\phi^2}{s-4m_e^2}}\left(1-\frac{4m_e^2}{s}\right), \quad (B3)$$

$$\sigma_{e^- e^+ \to \phi\phi}^{(Z')} = g_\phi^2(s-4m_\phi^2)\sqrt{\frac{s-4m_\phi^2}{s-4m_e^2}}$$
$$\times \frac{s(g_L^2+g_R^2)-m_e^2(g_L^2-6g_L g_R+g_R^2)}{96\pi s(s-m_{Z'}^2)^2}. \quad (B4)$$

3. $e - N$ bremsstrahlung

For the fixed-target experiments, we consider the production of ϕ pairs via electron-nucleus bremsstrahlung depicted in Fig. 5. Here, we need to compute the 2-to-4 cross section $\sigma_{2\to4}$ for the process $e^-(p_1) + N(p_2) \to e^-(p_3) + X_n(p_4) + \phi(p_\phi) + \phi^*(p_{\phi^*})$. We define $q = p_\phi + p_\phi^*$ with $q^2 \equiv s_{\phi\phi}$, $q_1 = p_1 - p_3$ with $q_1^2 \equiv t_1$, and $q_2 = p_2 - p_4$ with $q_2^2 \equiv t_2$ such that $q = q_1 + q_2$ given that total momentum is conserved. The differential cross section is then written as

$$d\sigma_{2\to4} = \frac{1}{4E_1 E_2 v_M} \frac{1}{g_1 g_2} \sum_{\text{spins}} |\mathcal{M}|^2 d\Phi, \tag{B5}$$

where g_1 and g_2 are spin degrees of freedom of electron and nucleus, respectively, while $|\mathcal{M}|^2$ is the amplitude square and $d\Phi$ is the total phase space. By introducing an integral with respect to $s_X \equiv m_X^2 = p_4^2$, in the lab frame Eq. (B5) becomes

$$d\sigma_{2\to4} = \frac{(4\pi\alpha)^2}{2|\vec{p}_1| m_N g_2 q_2^4} L^{\mu\nu,\rho\sigma} \phi_{\rho\sigma} W_{\mu\nu}(-q_2) ds_X d\Phi_4,$$

where $L^{\mu\nu,\rho\sigma}$ contains the leptonic average over g_1, $\phi_{\rho\sigma}$ includes the ϕ-emission piece together with the heavy mediator propagator, $W_{\mu\nu}$ is the hadronic tensor with its concrete form given in Ref. [68], and $d\Phi_4$ is the four-body phase space which is also analytically computed in Ref. [68].

The leptonic tensor from the two diagrams and their interference can be expressed as

$$L^{\mu\nu,\rho\sigma} = \frac{L_a^{\mu\nu,\rho\sigma}}{[(p_3 + q)^2 - m_e^2]^2} + \frac{L_b^{\mu\nu,\rho\sigma}}{[(p_1 - q)^2 - m_e^2]^2} + \frac{L_{ab}^{\mu\nu,\rho\sigma}}{[(p_3 + q)^2 - m_e^2][(p_1 - q)^2 - m_e^2]}, \tag{B6}$$

where, for completeness, we spell out the individual traces in the following. For the F-mediated model, they read

$$L_{a,F}^{\mu\nu,\rho\sigma} = \frac{1}{g_1 m_F^2} \text{Tr}[(\not{p}_3 + m_e)(c_L P_L + c_R P_R)(c_L P_R + c_R P_L)(\not{p}_3 + \not{q} + m_e)\gamma^\mu(\not{p}_1 + m_e)\gamma^\nu$$
$$\times (\not{p}_3 + \not{q} + m_e)(c_L P_L + c_R P_R)(c_L P_R + c_R P_L)],$$

$$L_{b,F}^{\mu\nu,\rho\sigma} = \frac{1}{g_1 m_F^2} \text{Tr}[(\not{p}_1 + m_e)(c_L P_L + c_R P_R)(c_L P_R + c_R P_L)(\not{p}_1 - \not{q} + m_e)\gamma^\nu(\not{p}_3 + m_e)\gamma^\mu$$
$$(\not{p}_1 - \not{q} + m_e)(c_L P_L + c_R P_R)(c_L P_R + c_R P_L)],$$

$$L_{ab,F}^{\mu\nu,\rho\sigma} = \frac{1}{g_1 m_F^2} \{\text{Tr}[(\not{p}_3 + m_e)(c_L P_L + c_R P_R)(c_L P_R + c_R P_L)(\not{p}_3 + \not{q} + m_e)\gamma^\mu(\not{p}_1 + m_e)(c_L P_L + c_R P_R)$$
$$(c_L P_R + c_R P_L)(\not{p}_1 - \not{q} + m_e)\gamma^\nu] + \text{Tr}[(\not{p}_3 + m_e)\gamma^\mu(\not{p}_1 - \not{q} + m_e)(c_L P_L + c_R P_R)(c_L P_R + c_R P_L)$$
$$(\not{p}_1 + m_e)\gamma^\nu(\not{p}_3 + \not{q} + m_e)(c_L P_L + c_R P_R)(c_L P_R + c_R P_L)]\}, \tag{B7}$$

where indices ρ, σ can obviously be abandoned. For the vector-mediated model, we obtain for the traces

$$L_{a,Z'}^{\mu\nu,\rho\sigma} = \frac{1}{g_1} \text{Tr}[(\not{p}_3 + m_e)\gamma^\rho(g_L P_L + g_R P_R)(\not{p}_3 + \not{q} + m_e)\gamma^\mu(\not{p}_1 + m_e)\gamma^\nu(\not{p}_3 + \not{q} + m_e)(g_L P_R + g_R P_L)\gamma^\sigma],$$

$$L_{b,Z'}^{\mu\nu,\rho\sigma} = \frac{1}{g_1} \text{Tr}[(\not{p}_1 + m_e)(g_L P_R + g_R P_L)\gamma^\sigma(\not{p}_1 - \not{q} + m_e)\gamma^\nu(\not{p}_3 + m_e)\gamma^\mu(\not{p}_1 - \not{q} + m_e)\gamma^\rho(g_L P_L + g_R P_R)],$$

$$L_{ab,Z'}^{\mu\nu,\rho\sigma} = \frac{1}{g_1} \{\text{Tr}[(\not{p}_3 + m_e)\gamma^\rho(g_L P_L + g_R P_R)(\not{p}_3 + \not{q} + m_e)\gamma^\mu(\not{p}_1 + m_e)(g_L P_R + g_R P_L)\gamma^\sigma(\not{p}_1 - \not{q} + m_e)\gamma^\nu]$$
$$+ \text{Tr}[(\not{p}_3 + m_e)\gamma^\mu(\not{p}_1 - \not{q} + m_e)\gamma^\rho(g_L P_L + g_R P_R)(\not{p}_1 + m_e)\gamma^\nu(\not{p}_3 + \not{q} + m_e)(g_L P_R + g_R P_L)\gamma^\sigma]\}. \tag{B8}$$

In the case that ϕ emission proceeds by F mediation, we may simplify the calculation by utilizing the fact that $m_F = 1$ TeV is much larger than any momentum transfer considered here and approximate the F propagator as

$$\frac{i(\not{q} + m_F)}{q^2 - m_F^2} \to \frac{-i}{m_F}, \tag{B9}$$

where q is the four-momentum flowing in the propagator. We, hence, write the $ll\phi\phi$ interaction as an effective operator suppressed by m_F. The ϕ-emission piece is thus $\phi_{\rho\sigma}^{(F)} = 1$, and the integral over the product of Lorentz-invariant phase space of ϕ and ϕ^* denoted by $d\Pi_{\phi,\phi^*}$ is given by

$$\int d\Pi_{\phi,\phi^*}(2\pi)^4\delta^{(4)}(q - p_\phi - p_{\phi^*})\phi_{\rho\sigma}^{(F)} = \frac{1}{8\pi}\sqrt{1 - \frac{4m_\phi^2}{s_{\phi\phi}}}.$$

Note that the Lorentz indices ρ, σ do not have physical meaning in the F-mediated model and are introduced to unify the notation of the two models.

The ϕ-emission piece $\phi_{\rho\sigma}^{(Z')}$ in the Z' case reads

$$\phi_{\rho\sigma}^{(Z')} = \frac{g_\phi^2}{(s_{\phi\phi} - m_{Z'}^2)^2}(q^\alpha q^\beta - 2p_\phi^\alpha p_{\phi^*}^\beta - 2p_{\phi^*}^\alpha p_\phi^\beta)\left(g_{\rho\alpha} - \frac{q_\rho q_\alpha}{m_{Z'}^2}\right)\left(g_{\sigma\beta} - \frac{q_\sigma q_\beta}{m_{Z'}^2}\right). \tag{B10}$$

Terms containing p_ϕ and p_{ϕ^*} can be integrated over the ϕ-pair phase space using a modified version of Lenard's formula [142] for massive final states, yielding

$$\int d\Pi_{\phi,\phi^*}(2\pi)^4\delta^{(4)}(q - p_\phi - p_{\phi^*})\phi_{\rho\sigma}^{(Z')} = \frac{1}{8\pi(s_{\phi\phi} - m_{Z'}^2)^2}\sqrt{1 - \frac{4m_\phi^2}{s_{\phi\phi}}}f_{Z'}(s_{\phi\phi})\left(-g_{\rho\sigma} + \frac{q_\rho q_\sigma}{s_{\phi\phi}}\right).$$

Here, the function $f(s_{\phi\phi})$ following the convention used in Refs. [68,142,158] and for the Z'-mediated model reads

$$f_{Z'}(s_{\phi\phi}) = \frac{1}{3}g_\phi^2 s_{\phi\phi}\left(1 - \frac{4m_\phi^2}{s_{\phi\phi}}\right). \tag{B11}$$

When considering the experiments NA64 and LDMX where final state electrons are measured, we utilize the following differential cross section:

$$\frac{d\sigma_{2\to4}^F}{dE_3 d\cos\theta_3} = \frac{\alpha^2}{8\pi^2 g_2 m_N}\sqrt{\frac{E_3^2 - m_e^2}{E_1^2 - m_e^2}}\int ds_X \int ds_{\phi\phi} \int dt_2 \int dp_{1q}\left|\frac{\partial\phi_4^{R4q}}{\partial p_{1q}}\right|\frac{1}{t_2^2}\frac{1}{\sqrt{\lambda(s_4, m_N^2, t_1)}}$$

$$\times L_F^{\mu\nu,\rho\sigma}W_{\mu\nu}(-q_2)\frac{1}{16\pi^2}\sqrt{1 - \frac{4m_\phi^2}{s_{\phi\phi}}}, \tag{B12}$$

$$\frac{d\sigma_{2\to4}^{Z'}}{dE_3 d\cos\theta_3} = \frac{\alpha^2}{8\pi^2 g_2 m_N}\sqrt{\frac{E_3^2 - m_e^2}{E_1^2 - m_e^2}}\int ds_X \int ds_{\phi\phi} \int dt_2 \int dp_{1q}\left|\frac{\partial\phi_4^{R4q}}{\partial p_{1q}}\right|\frac{1}{t_2^2}\frac{1}{\sqrt{\lambda(s_4, m_N^2, t_1)}}$$

$$\times L_{Z'}^{\mu\nu,\rho\sigma}W_{\mu\nu}(-q_2)\frac{1}{16\pi^2(s_{\phi\phi} - m_{Z'}^2)^2}\sqrt{1 - \frac{4m_\phi^2}{s_{\phi\phi}}}f_{Z'}(s_{\phi\phi})\left(-g_{\rho\sigma} + \frac{q_\rho q_\sigma}{s_{\phi\phi}}\right), \tag{B13}$$

where $p_{1q} \equiv p_1 \cdot q$, the angle ϕ_4^{R4q} is the angle between the $(\vec{q}_1, \vec{p}_1)$ plane and $(\vec{q}_1, \vec{q})$ plane in the frame that $\vec{p}_4 + \vec{q} = 0$, $s_4 \equiv (p_4 + q)^2 = (p_1 + p_2 - p_3)^2$, $\lambda(a, b, c) = a^2 + b^2 + c^2 - 2ab - 2bc - 2ac$ is the Källén function, and $E_1 = E_{\text{beam}}$ in the lab frame. The integration boundaries for $s_{\phi\phi}$, t_2, and p_{1q} and the Jacobian $|\partial\phi_4^{R4q}/\partial p_{1q}|$ are found in Refs. [68,142]. In the lab frame ($|\vec{p}_2| = 0$), the Lorentz-invariant variables s_4 and t_1 can be expressed in terms of E_1, E_3 and $\cos\theta_3$ as

$$s_4 = 2m_e^2 + m_N^2 + 2E_1 m_N - 2E_3 m_N - 2E_1 E_3 + 2\sqrt{E_1^2 - m_e^2}\sqrt{E_3^2 - m_e^2}\cos\theta_3,$$

$$t_1 = 2m_e^2 - 2E_1 E_3 + \sqrt{E_1^2 - m_e^2}\sqrt{E_3^2 - m_e^2}\cos\theta_3.$$

For the experiments mQ and BDX, we need the spectrum and distribution of the produced ϕ particles. Therefore, we use

$$
\frac{d\sigma_{2\to4}^{F,Z'}}{dE_\phi d\cos\theta_\phi} = \frac{\alpha^2}{16(2\pi)^5 g_2 m_N} \sqrt{\frac{E_\phi^2 - m_\phi^2}{E_1^2 - m_e^2}} \int ds_X \int ds_{36} \int dt_2 \int d\phi_{436}^* \int t_{23} \int d\phi_{36}^*
$$

$$
\times \frac{1}{t_2^2} \frac{1}{\sqrt{\lambda(s_{436}, m_N^2, t_{15})}} \frac{1}{\sqrt{\lambda(s_{36}, m_N^2, (p_1 - p_4 - p_\phi)^2)}} L_{F,Z'}^{\mu\nu,\rho\sigma} W_{\mu\nu}(-q_2) \phi_{\rho\sigma}^{(F,Z')}, \tag{B14}
$$

where $s_{36} \equiv (p_3 + p_{\phi^*})^2$, ϕ_{436}^* is the angle between the planes of $(\vec{p}_1 - \vec{p}_\phi, \vec{p}_1)$ and $(\vec{p}_1 - \vec{p}_\phi, \vec{p}_4)$ in the frame that $\vec{p}_3 + \vec{p}_4 + \vec{p}_{\phi^*} = 0$ ranging from 0 to 2π, $t_{23} \equiv (p_2 - p_3)^2$, ϕ_{36}^* is the angle between the planes of $(\vec{p}_1 - \vec{p}_4 - \vec{p}_\phi, \vec{p}_4)$ and $(\vec{p}_1 - \vec{p}_4 - \vec{p}_\phi, \vec{p}_3)$ in the frame that $\vec{p}_3 + \vec{p}_{\phi^*} = 0$ ranging from 0 to 2π, $s_{436} \equiv (p_3 + p_4 + p_{\phi^*})^2 = (p_1 + p_2 - p_\phi)^2$, and $t_{15} \equiv (p_1 - p_\phi)^2$. The integration boundaries of these variables are given in Ref. [68]. Note that

$$
(p_1 - p_4 - p_\phi)^2 = m_N^2 + s_X + s_{36} + t_{15} - s_{436} - t_2.
$$

In the lab frame, one obtains the relations

$$
s_{436} = m_e^2 + m_N^2 + m_\phi^2 + 2E_1 m_N - 2E_\phi m_N - 2E_1 E_\phi + 2\sqrt{E_1^2 - m_e^2}\sqrt{E_\phi^2 - m_\phi^2}\cos\theta_\phi,
$$

$$
t_{15} = m_e^2 + m_\phi^2 - 2E_1 E_\phi + 2\sqrt{E_1^2 - m_e^2}\sqrt{E_\phi^2 - m_\phi^2}\cos\theta_\phi.
$$

In the derivation of the squared amplitude, one needs to define an additional Lorentz-invariant variable $p_{65} \equiv p_{\phi^*} \cdot p_\phi$ so that every scalar product of momenta can be written in terms of a combination of Lorentz-invariant variables [68]. Using the fact that, in four-dimensional space-time, any five 4-vectors cannot be linearly independent, we express p_{65} as a function of other Lorentz-invariant variables by solving $\det(M) = 0$, where the (i, j) entry of the 5×5 matrix M is $p_i \cdot p_j$. There are two solutions of p_{65} corresponding to $\phi_{36}^* \in [0, \pi)$ and $\phi_{36}^* \in [\pi, 2\pi)$. Other Lorentz-invariant variables are not affected by $\phi_{36}^* \to 2\pi - \phi_{36}^*$.

4. $\phi - e$ scattering

To leading order, the differential recoil cross section $d\sigma_{\phi-e}/dE_R$ as a function of the incoming ϕ energy E_ϕ and the recoil energy of the electron, E_R, for the F (s- and u-channel scattering) and Z' (t-channel scattering) cases read as follows:

$$
\frac{d\sigma_{\phi-e}^F}{dE_R} = \frac{c_L^2 c_R^2 (E_R + 2m_e)}{4\pi(E_\phi^2 - m_\phi^2)m_F^2} \quad (m_{e,\phi} \ll m_F), \tag{B15}
$$

$$
\frac{d\sigma_{\phi-e}^{Z'}}{dE_R} = \frac{g_\phi^2 g_l^2 [2E_\phi m_e(E_\phi - E_R) - E_R m_\phi^2]}{4\pi(E_\phi^2 - m_\phi^2)(2E_R m_e + m_{Z'}^2)^2}, \tag{B16}
$$

where we use $g_L = g_R \equiv g_l$ for the sake of presenting a more compact formula. The equations above are used in computing the electron scattering signal in mQ and BDX.

To properly account for the Pauli blocking factor in the computation of the upper boundaries of the SN1987A exclusion region, we also provide the differential cross sections in terms of Mandelstam variable t, taking again the limit of heavy mediators:

$$
\frac{d\sigma_{\phi-e}^F}{dt} = \frac{c_L^2 c_R^2}{4\pi m_F^2} \frac{4m_e^2 - t}{(m_e^2 + m_\phi^2 - s)^2 - 4m_e^2 m_\phi^2}, \tag{B17}
$$

$$
\frac{d\sigma_{\phi-e}^{Z'}}{dt} = \frac{g_l^2 g_\phi^2}{4\pi m_{Z'}^4} \frac{(m_e^2 + m_\phi^2 - s)^2 + t(s - m_e^2)}{(m_e^2 + m_\phi^2 - s)^2 - 4m_e^2 m_\phi^2}. \tag{B18}
$$

APPENDIX C: FURTHER ONE-LOOP DIAGRAMS

The presence of heavy new charged fermions $F^\pm$ induces effective interactions between ϕ and SM gauge bosons through a set of triangle loops containing $F^\pm$ and SM charged leptons, demonstrated in Fig. 9. This loop-induced charge radius interaction can, e.g., be probed in direct detection experiments [48,159].

Here, we detail the calculation of the coupling of the ϕ pair to an off-shell photon via the aforementioned triangle loops. The amplitude that needs to be dotted into the off-shell photon reads

$$
i\mathcal{M}_{F,\mu} = \sum_l (i\mathcal{M}_{1F,\mu}^l + i\mathcal{M}_{2F,\mu}^l), \tag{C1}
$$

where $i\mathcal{M}_{1F,\mu}^l$ and $i\mathcal{M}_{2F,\mu}^l$ correspond to the diagrams containing one and two $F^\pm$ in the loop, respectively.

Note that we take one charged SM lepton as an example and denote its mass by m_l. Here, left- and right-handed SM leptons contribute equally, so we further set $c_L = c_R \equiv c_F$.

After using Feynman parametrization and dimensional regularization to perform the loop integral, we find that the divergences in $\mathcal{M}^l_{1F,\mu}$ and $\mathcal{M}^l_{2F,\mu}$ mutually cancel. The remaining finite terms read

$$i\mathcal{M}^l_{1F,\mu} = -i\frac{ec_F^2}{4\pi^2}\int_0^1 dz \int_0^{1-z} dx\left\{ p_{2,\mu}\left[\frac{m_l^2(z-1)+2m_l m_F z + m_\phi^2(z-1)z^2 + p^2 x(z+1)(x+z-1)}{\Delta_{1F}} + (3z+1)\ln\Delta_{1F}\right]\right.$$
$$\left. + p_\mu\left[\frac{m_l^2 x + m_l m_F(2x-1) + m_\phi^2 z(xz-z-2x+1) + p^2 x(x-1)(x+z-1)}{\Delta_{1F}} + (3x-2)\ln\Delta_{1F}\right]\right\}, \qquad (C2)$$

$$i\mathcal{M}^l_{2F,\mu} = i\frac{ec_F^2}{4\pi^2}\int_0^1 dz \int_0^{1-z} dx\left\{ p_{2,\mu}\left[\frac{m_F^2(z-1)+2m_l m_F z + m_\phi^2(z-1)z^2 + p^2 x(z+1)(x+z-1)}{\Delta_{2F}} + (3z+1)\ln\Delta_{2F}\right]\right.$$
$$\left. + p_\mu\left[\frac{m_F^2 x + m_l m_F(2x-1) + m_\phi^2 z(xz-z-2x+1) + p^2 x(x-1)(x+z-1)}{\Delta_{2F}} + (3x-2)\ln\Delta_{2F}\right]\right\}, \qquad (C3)$$

with p_μ being the four-momentum of the photon, $p_{2,\mu}$ the four-momentum of one of the outgoing ϕ particles, and

$$\Delta_{1F} = -m_l^2(z-1) + z[m_F^2 + m_\phi^2(z-1)] + p^2 x(x+z-1),$$
$$\Delta_{2F} = -m_F^2(z-1) + z[m_l^2 + m_\phi^2(z-1)] + p^2 x(x+z-1).$$

Note that, if $m_l = m_F$, the total amplitude vanishes, as a manifestation of Furry's theorem. One can also directly write the combination of the two diagrams as an effective charge radius operator if we integrate out the heavy F:

$$-b_\phi \partial_\mu \phi \partial_\nu \phi^* F^{\mu\nu}, \qquad (C4)$$

where $F^{\mu\nu}$ is the field strength tensor of SM photon. We have checked that our loop calculation correctly matches onto this effective operator, with the Wilson coefficient

$$b_\phi = \frac{ec_F^2}{4\pi^2}\int_0^1 dz \int_0^{1-z} dx\left\{\frac{x(x+z-1)[m_l^2(z^2+z-2)+2m_l m_F z - z(z+1)m_F^2 - z(z-1)m_\phi^2]}{[m_l^2(z-1)-zm_F^2-z(z-1)m_\phi^2]^2} - (m_l \leftrightarrow m_F)\right\}, \qquad (C5)$$
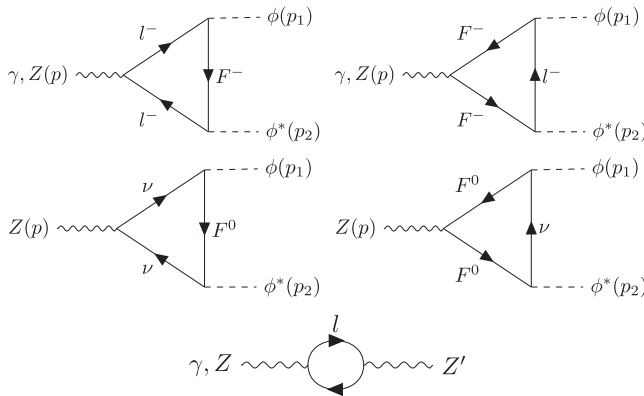

FIG. 9.   Top: triangle loop coupling ϕ to Z or γ with one charged F (left) and two charged F (right). Middle: triangle loop coupling ϕ to Z with one (left) or two (right) neutral F states. Bottom: loop-induced $\gamma - Z'$ and $Z - Z'$ mixing (which also contributes to the coupling to a ϕ pair).

in numerical agreement with previous results [48,159]. Note that a sum over the contributions from all SM leptons needs to be performed in the actual evaluation.

The above calculation can be generalized to infer the additional contribution to the invisible Z decay width by replacing the relevant couplings in the above amplitudes by the weak charges

$$e \to \frac{e}{2s_W c_W}g_V, \qquad (C6)$$

where $s_W = \sin\theta_W$ and $c_W = \cos\theta_W$ with θ_W being the weak angle and g_V being the usual vector coupling of weak current; axial vector currents do not contribute when $c_L = c_R$. Note that one also needs to include the contribution from diagrams containing neutral leptons as shown in the bottom panel in Fig. 9. We have checked that the resulting bound on c_F is rather weak and is, thus, not shown in the constraint plots.

In the Z' case, the SM photon or Z boson gains an effective coupling to ϕ via mixing with Z', originating from a SM lepton loop, shown in the bottom panel in Fig. 9. To estimate the mixing, we need to compute the polarization mixing tensor $i\Pi^{\mu\nu}$ given by the usual Lorentz structure, $i\Pi^{\mu\nu} = i(p^2 g^{\mu\nu} - p^\mu p^\nu)\Pi(p^2)$. For the SM photon and taking $g_L = g_R \equiv g_l$, we find in dimensional regularization the mixing self-energy

$$\Pi(p^2) = -\frac{eg_l}{2\pi^2}\int_0^1 dx\, x(1-x)\left[\frac{2}{\epsilon} + \ln\frac{\tilde{\mu}^2}{\Delta} + \mathcal{O}(\epsilon)\right], \quad (C7)$$

where ϵ is an infinitesimal number, $\tilde{\mu}^2 = 4\pi e^{-\gamma_E}\mu^2$ with γ_E the Euler-Mascheroni constant, μ the renormalization scale, and $\Delta = m_l^2 - x(1-x)p^2$.

Equivalently, one can also rewrite the self-energy of Eq. (C7) in terms of the standard Passarino-Veltman integrals [160–162] as

$$\Pi(p^2) = \frac{eg_l}{12\pi^2 p^2}[2A_0(m_l^2) - (p^2 + 2m_l^2)B_0(p^2, m_l^2, m_l^2)]. \tag{C8}$$

The divergence in $\Pi(p^2)$ can be canceled by a counterterm; that is, after specifying a renormalization condition, the effective mixing can be evaluated. The mixing between Z and Z' is computed in the same way but with Eq. (C6). Nevertheless, the ensuing constraint on $\sqrt{g_\phi g_l}$ from the Z invisible decay is fully covered by the LEP bound.

---

[1] P. Hut, Phys. Lett. **69B**, 85 (1977).
[2] B. W. Lee and S. Weinberg, Phys. Rev. Lett. **39**, 165 (1977).
[3] C. Boehm, T. Ensslin, and J. Silk, J. Phys. G **30**, 279 (2004).
[4] C. Boehm and P. Fayet, Nucl. Phys. **B683**, 219 (2004).
[5] P. Fayet, Phys. Lett. **95B**, 285 (1980).
[6] P. Fayet, Nucl. Phys. **B187**, 184 (1981).
[7] P. Jean et al., Astron. Astrophys. **407**, L55 (2003).
[8] J. Knodlseder et al., Astron. Astrophys. **411**, L457 (2003).
[9] N. Prantzos et al., Rev. Mod. Phys. **83**, 1001 (2011).
[10] T. Siegert, R. Diehl, G. Khachatryan, M. G. Krause, F. Guglielmetti, J. Greiner, A. W. Strong, and X. Zhang, Astron. Astrophys. **586**, A84 (2016).
[11] C. Boehm, D. Hooper, J. Silk, M. Casse, and J. Paul, Phys. Rev. Lett. **92**, 101301 (2004).
[12] J. F. Beacom, N. F. Bell, and G. Bertone, Phys. Rev. Lett. **94**, 171301 (2005).
[13] Y. Rasera, R. Teyssier, P. Sizun, B. Cordier, J. Paul, M. Casse, and P. Fayet, Phys. Rev. D **73**, 103518 (2006).
[14] F. H. Panther, R. M. Crocker, Y. Birnboim, I. R. Seitenzahl, and A. J. Ruiter, Mon. Not. R. Astron. Soc. **474**, L17 (2018).
[15] P. Fayet, Phys. Lett. B **172**, 363 (1986).
[16] C. Boehm and Y. Ascasibar, Phys. Rev. D **70**, 115013 (2004).
[17] C. Boehm and P. Uwer, arXiv:hep-ph/0606058.
[18] R. J. Wilkinson, A. C. Vincent, C. Boehm, and C. McCabe, Phys. Rev. D **94**, 103525 (2016).
[19] G. Bennett et al. (Muon g-2 Collaboration), Phys. Rev. D **73**, 072003 (2006).
[20] F. Jegerlehner and A. Nyffeler, Phys. Rep. **477**, 1 (2009).
[21] M. Pospelov, Phys. Rev. D **80**, 095002 (2009).
[22] B. Moore, Nature (London) **370**, 629 (1994).
[23] R. A. Flores and J. R. Primack, Astrophys. J. Lett. **427**, L1 (1994).

[24] D. N. Spergel and P. J. Steinhardt, Phys. Rev. Lett. **84**, 3760 (2000).
[25] L. Goodenough and D. Hooper, arXiv:0910.2998.
[26] M. Pospelov and A. Ritz, Phys. Lett. B **671**, 391 (2009).
[27] N. Arkani-Hamed, D. P. Finkbeiner, T. R. Slatyer, and N. Weiner, Phys. Rev. D **79**, 015014 (2009).
[28] D. Hooper and L. Goodenough, Phys. Lett. B **697**, 412 (2011).
[29] R. Essig et al., in Community Summer Study 2013: Snowmass on the Mississippi (SLAC National Accelerator Laboratory, 2013) [arXiv:1311.0029].
[30] J. Alexander et al., arXiv:1608.08632.
[31] M. Battaglieri et al., in U.S. Cosmic Visions: New Ideas in Dark Matter (California Digital Library, 2017) [arXiv:1707.04591].
[32] R. H. Parker, C. Yu, W. Zhong, B. Estey, and H. Müller, Science **360**, 191 (2018).
[33] L. Morel, Z. Yao, P. Cladé, and S. Guellati-Khélifa, Nature (London) **588**, 61 (2020).
[34] Y. Ascasibar, P. Jean, C. Boehm, and J. Knoedlseder, Mon. Not. R. Astron. Soc. **368**, 1695 (2006).
[35] A. C. Vincent, P. Martin, and J. M. Cline, J. Cosmol. Astropart. Phys. 04 (2012) 022.
[36] J. C. Higdon, R. E. Lingenfelter, and R. E. Rothschild, Astrophys. J. **698**, 350 (2009).
[37] R. E. Lingenfelter, J. C. Higdon, and R. E. Rothschild, Phys. Rev. Lett. **103**, 031301 (2009).
[38] C. A. Kierans et al., arXiv:1903.05569.
[39] M. Boudaud, J. Lavalle, and P. Salati, Phys. Rev. Lett. **119**, 021103 (2017).
[40] J. F. Beacom and H. Yuksel, Phys. Rev. Lett. **97**, 071102 (2006).
[41] P. Sizun, M. Casse, and S. Schanne, Phys. Rev. D **74**, 063514 (2006).
[42] M. Cirelli, N. Fornengo, B. J. Kavanagh, and E. Pinetti, arXiv:2007.11493.

[43] R. Bartels, D. Gaggero, and C. Weniger, J. Cosmol. Astropart. Phys. 05 (2017) 001.

[44] P. Agrawal, S. Blanchet, Z. Chacko, and C. Kilic, Phys. Rev. D **86**, 055002 (2012).

[45] D. Schmidt, T. Schwetz, and T. Toma, Phys. Rev. D **85**, 073009 (2012).

[46] Y. Zhang, Phys. Lett. B **720**, 137 (2013).

[47] Y. Bai and J. Berger, J. High Energy Phys. 11 (2013) 171.

[48] Y. Bai and J. Berger, J. High Energy Phys. 08 (2014) 153.

[49] P. Agrawal, B. Batell, D. Hooper, and T. Lin, Phys. Rev. D **90**, 063512 (2014).

[50] J. Kile, A. Kobach, and A. Soni, Phys. Lett. B **744**, 330 (2015).

[51] D. Egana-Ugrinovic, M. Low, and J. T. Ruderman, J. High Energy Phys. 05 (2018) 012.

[52] J. P. Leveille, Nucl. Phys. **B137**, 63 (1978).

[53] T. Toma, Phys. Rev. Lett. **111**, 091301 (2013).

[54] F. Giacchino, L. Lopez-Honorez, and M. H. Tytgat, J. Cosmol. Astropart. Phys. 10 (2013) 025.

[55] F. Giacchino, L. Lopez-Honorez, and M. H. Tytgat, J. Cosmol. Astropart. Phys. 08 (2014) 046.

[56] C. Boehm, Y. Farzan, T. Hambye, S. Palomares-Ruiz, and S. Pascoli, Phys. Rev. D **77**, 043516 (2008).

[57] N. Aghanim et al. (Planck Collaboration), Astron. Astrophys. **641**, A6 (2020).

[58] P. Langacker, Rev. Mod. Phys. **81**, 1199 (2009).

[59] P. J. Fox and E. Poppitz, Phys. Rev. D **79**, 083528 (2009).

[60] X.-J. Bi, X.-G. He, and Q. Yuan, Phys. Lett. B **678**, 168 (2009).

[61] N. F. Bell, Y. Cai, R. K. Leane, and A. D. Medina, Phys. Rev. D **90**, 035027 (2014).

[62] C. Boehm and J. Silk, Phys. Lett. B **661**, 287 (2008).

[63] P. Agrawal, Z. Chacko, and C. B. Verhaaren, J. High Energy Phys. 08 (2014) 147.

[64] S. Bilmis, I. Turan, T. Aliev, M. Deniz, L. Singh, and H. Wong, Phys. Rev. D **92**, 033009 (2015).

[65] M. Cadeddu, N. Cargioli, F. Dordei, C. Giunti, Y. Li, E. Picciau, and Y. Zhang, J. High Energy Phys. 01 (2021) 116.

[66] M. Ibe, H. Murayama, and T. Yanagida, Phys. Rev. D **79**, 095009 (2009).

[67] J. M. Cline, H. Liu, T. Slatyer, and W. Xue, Phys. Rev. D **96**, 083521 (2017).

[68] X. Chu, J. Pradler, and L. Semmelrock, Phys. Rev. D **99**, 015040 (2019).

[69] B. Aubert et al. (BABAR Collaboration), Nucl. Instrum. Methods Phys. Res., Sect. A **479**, 1 (2002).

[70] D. Banerjee et al. (NA64 Collaboration), Phys. Rev. D **97**, 072002 (2018).

[71] S. Gninenko (NA64 Collaboration), NA64 Status Report 2020, Technical Report No. CERN-SPSC-2020-017. SPSC-SR-273, CERN, Geneva, 2020.

[72] A. A. Prinz et al., Phys. Rev. Lett. **81**, 1175 (1998).

[73] A. A. Prinz, Ph.D. thesis, Stanford University, Physics Department, 2001.

[74] A. Abashian et al., Nucl. Instrum. Methods Phys. Res., Sect. A **479**, 117 (2002).

[75] T. Abe et al. (Belle-II Collaboration), arXiv:1011.0352.

[76] J. Mans (LDMX Collaboration), EPJ Web Conf. **142**, 01020 (2017).

[77] M. Battaglieri et al. (BDX Collaboration), arXiv:1712.01518.

[78] R. Essig, J. Mardon, M. Papucci, T. Volansky, and Y.-M. Zhong, J. High Energy Phys. 11 (2013) 167.

[79] M. Battaglieri et al. (BDX Collaboration), arXiv:1910.03532.

[80] P. Achard et al. (L3 Collaboration), Phys. Lett. B **587**, 16 (2004).

[81] F. Rossi-Torres and C. Moura, Phys. Rev. D **92**, 115022 (2015).

[82] P. J. Fox, R. Harnik, J. Kopp, and Y. Tsai, Phys. Rev. D **84**, 014028 (2011).

[83] K. Cheung, P.-Y. Tseng, Y.-L. S. Tsai, and T.-C. Yuan, J. Cosmol. Astropart. Phys. 05 (2012) 001.

[84] P. Ilten, Y. Soreq, M. Williams, and W. Xue, J. High Energy Phys. 06 (2018) 004.

[85] A. Freitas and S. Westhoff, J. High Energy Phys. 10 (2014) 116.

[86] A. Freitas, J. Lykken, S. Kell, and S. Westhoff, J. High Energy Phys. 05 (2014) 145; 09 (2014) 155(E).

[87] F. del Aguila, M. Chala, J. Santiago, and Y. Yamamoto, J. High Energy Phys. 03 (2015) 059.

[88] N. Chen, J. Wang, and X.-P. Wang, arXiv:1501.04486.

[89] D. Hanneke, S. Fogwell, and G. Gabrielse, Phys. Rev. Lett. **100**, 120801 (2008).

[90] M. Tanabashi et al. (Particle Data Group), Phys. Rev. D **98**, 030001 (2018).

[91] P. Zyla et al. (Particle Data Group), Prog. Theor. Exp. Phys. **2020**, 083C01 (2020).

[92] M. Bouchiat and C. Bouchiat, Rep. Prog. Phys. **60**, 1351 (1997).

[93] C. Bouchiat and P. Fayet, Phys. Lett. B **608**, 87 (2005).

[94] P. Fayet, Eur. Phys. J. C **77**, 53 (2017).

[95] A. Czarnecki and W. J. Marciano, Int. J. Mod. Phys. A **15**, 2365 (2000).

[96] P. Anthony et al. (SLAC E158 Collaboration), Phys. Rev. Lett. **95**, 081601 (2005).

[97] J. Benesch et al. (MOLLER Collaboration), arXiv:1411.4088.

[98] D. Becker et al., arXiv:1802.04759.

[99] K. Kumar, S. Mantry, W. Marciano, and P. Souder, Annu. Rev. Nucl. Part. Sci. **63**, 237 (2013).

[100] G. Arcadi, M. Lindner, J. Martins, and F. S. Queiroz, Nucl. Phys. **B959**, 115158 (2020).

[101] Y. Kuno and Y. Okada, Rev. Mod. Phys. **73**, 151 (2001).

[102] A. Baldini et al. (MEG Collaboration), Eur. Phys. J. C **76**, 434 (2016).

[103] S. Esch, M. Klasen, D. R. Lamprea, and C. E. Yaguna, Eur. Phys. J. C **78**, 88 (2018).

[104] F. Renga, Rev. Phys. **4**, 100029 (2019).

[105] H. Davoudiasl, H.-S. Lee, and W. J. Marciano, Phys. Rev. D **85**, 115019 (2012).

[106] F. D'Eramo, B. J. Kavanagh, and P. Panci, Phys. Lett. B **771**, 339 (2017).

[107] G. Steigman, J. Cosmol. Astropart. Phys. 04 (2010) 029.

[108] G. Mangano and P. D. Serpico, Phys. Lett. B **701**, 296 (2011).

[109] J. Hamann, S. Hannestad, G. G. Raffelt, and Y. Y. Wong, J. Cosmol. Astropart. Phys. 09 (2011) 034.

[110] C. Boehm, M. J. Dolan, and C. McCabe, J. Cosmol. Astropart. Phys. 08 (2013) 041.

[111] J. H. Heo and C. Kim, J. Korean Phys. Soc. **68**, 715 (2016).

[112] N. Fornengo, C. Kim, and J. Song, Phys. Rev. D **56**, 5123 (1997).

[113] M. Escudero, J. Cosmol. Astropart. Phys. 02 (2019) 007.

[114] P. F. Depta, M. Hufnagel, K. Schmidt-Hoberg, and S. Wild, J. Cosmol. Astropart. Phys. 04 (2019) 029.

[115] N. Sabti, J. Alvey, M. Escudero, M. Fairbairn, and D. Blas, J. Cosmol. Astropart. Phys. 01 (2020) 004.

[116] R. Essig, J. Mardon, and T. Volansky, Phys. Rev. D **85**, 076007 (2012).

[117] L. Barak et al. (SENSEI Collaboration), Phys. Rev. Lett. **125**, 171802 (2020).

[118] R. Essig, A. Manalaysay, J. Mardon, P. Sorensen, and T. Volansky, Phys. Rev. Lett. **109**, 021301 (2012).

[119] R. Essig, T. Volansky, and T.-T. Yu, Phys. Rev. D **96**, 043017 (2017).

[120] E. Aprile et al. (XENON Collaboration), Phys. Rev. Lett. **123**, 251801 (2019).

[121] H. An, M. Pospelov, J. Pradler, and A. Ritz, Phys. Rev. Lett. **120**, 141801 (2018); **121**, 259903(E) (2018).

[122] M. Hufnagel, K. Schmidt-Hoberg, and S. Wild, J. Cosmol. Astropart. Phys. 02 (2018) 044.

[123] H. Liu, T. R. Slatyer, and J. Zavala, Phys. Rev. D **94**, 063507 (2016).

[124] E. C. Stone, A. C. Cummings, F. B. McDonald, B. C. Heikkila, N. Lal, and W. R. Webber, Science **341**, 150 (2013).

[125] M. Boudaud, T. Lacroix, M. Stref, and J. Lavalle, Phys. Rev. D **99**, 061302 (2019).

[126] A. De Angelis et al. (e-ASTROGAM Collaboration), Exp. Astron. **44**, 25 (2017).

[127] R. Caputo et al. (AMEGO Collaboration), arXiv:1907.07558.

[128] C. Boehm, P. Fayet, and R. Schaeffer, Phys. Lett. B **518**, 8 (2001).

[129] C. Boehm and R. Schaeffer, Astron. Astrophys. **438**, 419 (2005).

[130] R. J. Wilkinson, C. Boehm, and J. Lesgourgues, J. Cosmol. Astropart. Phys. 05 (2014) 011.

[131] A. Arhrib, C. Bœhm, E. Ma, and T.-C. Yuan, J. Cosmol. Astropart. Phys. 04 (2016) 049.

[132] X. Chu, C. Garcia-Cely, and T. Hambye, J. High Energy Phys. 11 (2016) 048.

[133] S. W. Randall, M. Markevitch, D. Clowe, A. H. Gonzalez, and M. Bradac, Astrophys. J. **679**, 1173 (2008).

[134] D. Harvey, R. Massey, T. Kitching, A. Taylor, and E. Tittley, Science **347**, 1462 (2015).

[135] A. Robertson, R. Massey, and V. Eke, Mon. Not. R. Astron. Soc. **465**, 569 (2017).

[136] D. Harvey, A. Robertson, R. Massey, and I. G. McCarthy, Mon. Not. R. Astron. Soc. **488**, 1572 (2019).

[137] K. Bondarenko, A. Boyarsky, T. Bringmann, and A. Sokolenko, J. Cosmol. Astropart. Phys. 04 (2018) 049.

[138] G. G. Raffelt, Stars as Laboratories for Fundamental Physics (University of Chicago Press, Chicago, 1996).

[139] N. Bar, K. Blum, and G. D'Amico, Phys. Rev. D **101**, 123025 (2020).

[140] D. Page, M. V. Beznogov, I. Garibay, J. M. Lattimer, M. Prakash, and H.-T. Janka, Astrophys. J. **898**, 125 (2020).

[141] J. H. Chang, R. Essig, and S. D. McDermott, J. High Energy Phys. 09 (2018) 051.

[142] X. Chu, J.-L. Kuo, J. Pradler, and L. Semmelrock, Phys. Rev. D **100**, 083002 (2019).

[143] T. Fischer, S. Chakraborty, M. Giannotti, A. Mirizzi, A. Payez, and A. Ringwald, Phys. Rev. D **94**, 085012 (2016).

[144] P. Fayet, D. Hooper, and G. Sigl, Phys. Rev. Lett. **96**, 211302 (2006).

[145] A. Guha, P. B. Dev, and P. K. Das, J. Cosmol. Astropart. Phys. 02 (2019) 032.

[146] L. Darmé, S. A. Ellis, and T. You, J. High Energy Phys. 07 (2020) 053.

[147] J. Beacham et al., J. Phys. G **47**, 010501 (2020).

[148] T. Emken, R. Essig, C. Kouvaris, and M. Sholapurkar, J. Cosmol. Astropart. Phys. 09 (2019) 070.

[149] N. F. Bell, G. Busoni, and S. Robles, J. Cosmol. Astropart. Phys. 06 (2019) 054.

[150] R. Garani and J. Heeck, Phys. Rev. D **100**, 035039 (2019).

[151] R. Garani, A. Gupta, and N. Raj, Phys. Rev. D **103**, 043019 (2021).

[152] A. Berlin, N. Blinov, G. Krnjaic, P. Schuster, and N. Toro, Phys. Rev. D **99**, 075001 (2019).

[153] T. Åkesson et al. (LDMX Collaboration), arXiv:1808.05219.

[154] L. Doria, P. Achenbach, M. Christmann, A. Denig, P. Gülker, and H. Merkel, in 13th Conference on the Intersections of Particle and Nuclear Physics (SLAC National Accelerator Laboratory, 2018) [arXiv:1809.07168].

[155] R. Mertig, M. Bohm, and A. Denner, Comput. Phys. Commun. **64**, 345 (1991).

[156] V. Shtabovenko, R. Mertig, and F. Orellana, Comput. Phys. Commun. **207**, 432 (2016).

[157] P. Gondolo and G. Gelmini, Nucl. Phys. **B360**, 145 (1991).

[158] X. Chu, J.-L. Kuo, and J. Pradler, Phys. Rev. D **101**, 075035 (2020).

[159] A. Hamze, C. Kilic, J. Koeller, C. Trendafilova, and J.-H. Yu, Phys. Rev. D **91**, 035009 (2015).

[160] G. Passarino and M. Veltman, Nucl. Phys. **B160**, 151 (1979).

[161] G. 't Hooft and M. Veltman, Nucl. Phys. **B153**, 365 (1979).

[162] T. Hahn, Nucl. Phys. B, Proc. Suppl. **89**, 231 (2000).